Engineering Geology 128 (2012) 30–48

Contents lists available at ScienceDirect

Engineering Geology

journal homepage: www.elsevier.com/locate/enggeo

Characterization of the 3D geometry of flow-like landslides: A methodology based on the integration of heterogeneous multi-source data

J. Travelletti [a,b,*], J.-P. Malet [a]

[a] Institut de Physique du Globe de Strasbourg, CNRS UMR 7516, University of Strasbourg, 5 rue René Descartes, F-67084 Strasbourg Cedex, France
[b] GEOPHEN - LETG, CNRS UMR 6554, University of Caen Basse-Normandie, Esplanade de la Paix, F-14032 Caen Cedex, France

ARTICLE INFO

Article history:
Received 14 July 2010
Received in revised form 13 April 2011
Accepted 3 May 2011
Available online 10 May 2011

Keywords:
Landslide
3D geometry
Multi-source data integration
Geostatistical model

ABSTRACT

The geometry of the bedrock, internal layers and slip surfaces control the deformation pattern and the mechanisms of landslides. A challenge to progress in understanding landslide behavior is to construct accurate 3D geometrical models from different surveying techniques. The objective of this work is to present a methodology for integrating multi-source and multi-resolution data in a 3D geometrical model using geostatistical tools. The methodology consists in integrating the data by extracting relevant information on the internal structure of the landslide and in detecting possible incoherencies between different interpretations. A simple method to classify the input data and to control their influence on the model interpolation is proposed through the development of an expert reliability index. The methodology is applied for the creation of a 3D geometrical model of the Super-Sauze mudslide (South French Alps) for which an extensive dataset is available. Error calculation and expert geomorphological interpretation allow one to select the most suitable interpolation algorithm and to define the volumes of each layer. The proposed 3D geometrical model highlights the influence of the bedrock geometry on the observed kinematic pattern.

1. Introduction

The geometry of the bedrock, internal layers and slip surfaces of landslides controls their deformation pattern and mechanisms (Malet et al., 2002; Schulz et al., 2009; Crozier, 2010). The development of extension and compression zones within the landslide, the generation of excess pore water pressure and differential displacements at the ground surface are major effects resulting from the sub-surface topography (Savage and Smith, 1986; Picarelli et al., 1995; Picarelli, 2001; van Asch et al., 2006). Therefore, the characterization of the 3D internal structure is a pre-requisite to any slope stability analysis and hydro-mechanical modeling (Brunsden, 1999; Savage and Wasowski, 2006; Travelletti et al., 2009).

Significant developments in both direct and indirect sub-surface investigations were realized in the last decades to define the features of a landslide (Turner and Schuster, 1996; Cornforth, 2005). The choice of an appropriate sub-surface exploration method mainly depends on the site configuration, material characteristics, time and economic constraints. Therefore, complementary methods have been applied to provide indirect and spatially-distributed information of the 3D sub-surface structure such as 2D and 3D geophysical tomographies (Jongmans and Garambois, 2007) and remote-sensing techniques (LiDAR, InSAR; Delacourt et al., 2007) in combination with classical geotechnical investigations. Because these multi-source data have heterogeneous qualities and different spatial resolutions, a major difficulty in 3D geometrical modeling consists in the extraction of relevant information and in their integration in a coherent framework (Bichler et al., 2004; Regli et al., 2004; Caumon et al., 2009). Consequently, before incorporating the data in a 3D geometrical model, several pre-processing steps are necessary. The data quality has to be carefully checked because it directly affects the final quality of the geometrical model. Evans (2003) distinguished two major types of uncertainty in 3D geometrical modeling: those affecting data and measurements themselves and those resulting from the modeling process. Therefore identifying which amount of data is reliable is important to weight their effects on the geometrical model. The problem is that, in most cases, typical data for 3D geometrical modeling are already in an interpretive digital or numerical form (e.g. maps, cross-sections) for which the uncertainty is very difficult to assess without access to the raw data. Poeter and Mckenna (1995) and Clarke (2004) define a very simple and general approach to assess the quality of the data by introducing the concepts of "hard data" and "soft data" and the development of a reliability index. "Hard data" are defined by explicit properties and low uncertainties on the layering geometry of the landslide (e.g. stratigraphic logs, landslide boundary defined from geomorphologic observations); "Soft data" are defined by implicit properties and higher uncertainties. Such data need consequently several processing steps before the extraction of useful information on the geometry (e.g. filtering, inversion, information derived from empirical or analytical relationships; Regli et al., 2004; Gallerini and De Donatis, 2009).

* Corresponding author at: Institut de Physique du Globe de Strasbourg, CNRS UMR 7516, University of Strasbourg, 5 rue René Descartes, F-67084 Strasbourg Cedex, France. Tel.: +33 3 68 85 00 36; fax: +33 3 68 85 01 25.
E-mail address: julien.travelletti@unistra.fr (J. Travelletti).

0013-7952/$ – see front matter © 2011 Elsevier B.V. All rights reserved.
doi:10.1016/j.enggeo.2011.05.003

The quality of the 3D geometrical modeling can be defined by applying statistical methods such as the comparison of several models created from the same initial dataset (Regli et al., 2004, Caumon, 2010) and analysis of the Root Mean Square Error (Desmet, 1997; Aguilar et al., 2005; Weng, 2006), and empirical methods such as global visualization of the sub-surface topography and expert analysis (Aguilar et al., 2005, Fisher and Tate, 2006).

Regarding the diversity of landslide geometries, attempting to provide a methodology for 3D landslide modeling is a real challenge. This work is essentially focused on landslides whose basal shear surface is continuous. First a review of the data sources used for geometrical modeling of landslides is presented. Second the methodology is detailed. It consists of several stages of data integration (georeferencing, (re-)interpretation of the data, information extraction and detection of possible incoherencies among the different interpretations). A simple method for classifying the input data is then presented. Third the methodology is applied to the construction of the 3D geometry of the Super-Sauze mudslide (Barcelonnette Basin, South French Alps) using two geostatistical modeling packages (*RockWork©*, Rockworks, 2004; *Surfer© v 8.01*, Golden software, 2002). Four interpolation algorithms are tested and several criteria and validation methods are presented for selecting the most suitable 3D geometrical model for slope stability analyses and hydro-mechanical modeling. Finally, the influence of data point density and temporal resolution on the coherency of the 3D geometrical model is discussed.

2. Sources of data

The 3D geometrical modeling of landslides first starts with the collection of data which contain geometrical information at the ground surface (typically landslide boundaries) and information on the internal structure geometry. Because the choice of the sub-surface investigations techniques is not the purpose of this study, the authors refer the reader to well-documented references such as Sowers and Royster (1978), Turner and Schuster (1996) and Cornforth (2005). From a practical point of view, data collection and field investigation must be extended beyond the landslide area for two main reasons:

- to ensure that the entire landslide area is included; experience indicates that the landslide area is generally much larger than first suspected and tends to enlarge through time;
- to detect property anomalies in the data acquired in- and outside the landslide.

Five major sources of data can be used: kinematic data, geomorphologic data, geological data, geotechnical data and petro-physical data (Table 1). Each data type has its own spatial extension and resolution. They can be determined by direct or indirect measurements. Indirect data has the advantage to provide spatially distributed information, but the resolution and accuracy are generally lower than direct and punctual data.

- *Kinematic data:* these data are used to delimit the landslide extension both in depth and at the surface. When the identification of internal shear zones is not obvious in geological records, inclinometer data are common to localize internal shear zones (Cornforth, 2005). Traditional and punctual geodetic techniques (e.g. extensometers, GPS, tacheometry; Angeli et al., 2000; Malet et al., 2002) and remote-sensing techniques (e.g. DInSAR, correlation of satellite, aerial and terrestrial images, airborne and terrestrial LiDAR; Casson et al. 2003; Squarzoni et al., 2003; Delacourt et al., 2007; Teza et al., 2008; Travelletti et al., 2008; Oppikofer et al., 2009) can be used to define the landslide spatial boundaries. Digital Elevation Models (DEMs) can usually be derived from these techniques, and multi-temporal analysis allow one to highlight limits between areas affected by elevation changes. Although the interpretation of displacement data is, in most cases very reliable to establish landslide boundaries, the real landslide extension may be underestimated if a part of the landslide is in a dormant stage of activity (Cruden and Varnes, 1996).
- *Geomorphologic data:* because the geometry of the ground surface is an overt clue to landslide activity (Sowers and Royster, 1978), landform evolution can be used to determine the landslide boundaries.

Table 1
Type of data sources and associated investigation techniques able to provide information on landslide geometry.

Data type	Type of techniques	Type of information[a]	Spatial extension	Typical resolution
Kinematic	Inclinometers	Internal	1D	10^{-3}–10^{-2} m
	Extensometers	Surface	1D	10^{-3}–10^{-2} m
	GPS monitoring	Surface	1D	10^{-3}–10^{-2} m
	Tacheometry monitoring	Surface	1D	10^{-3}–10^{-2} m
	Differential photogrammetric DEMs	Surface	2D–2.5D	10^{-2}–10^{0} m
	Differential terrestrial and airborne LiDAR survey	Surface	2D–2.5D	10^{-2} m
	Differential InSAR survey	Surface	2D–2.5D	10^{-3}–10^{-2} m
	Image correlation of (ortho)photographs	Surface	2D–2.5D	10^{-2}–10^{0} m
Geomorphological	Oblique photographs from the air or from the ground	Surface	2D	10^{-2} m
	Aerial and satellite orthophotographs	Surface	2D	10^{-2}–10^{1} m
	Photogrammetric DEM	Surface	2.5D	10^{-2}–10^{1} m
	Terrestrial and airborne LiDAR (DEM)	Surface	2.5D	10^{-2} m
	InSAR (DEM)	Surface	2.5D	10^{-3}–10^{-2} m
Geological	Geological mapping	Surface	2D	10^{1}–10^{1} m
	Boreholes stratigraphic logs in (non)destructive drilling	Internal	1D	10^{-2}–10^{-1} m
	test pits, trenches	Internal	1D	Variable
Geotechnical	Pressiometric tests	Internal	1D	10^{-2}–10^{0} m
	Static or dynamic penetration tests	Internal	1D	10^{-2}–10^{-1} m
	Field van tests	Internal	1D	10^{-2}–10^{-1} m
Petro-physical	Seismic reflection	Internal	2D–3D	10^{-1}–10^{0} m
	Seismic refraction tomography	Internal	2D–3D	10^{-1}–10^{0} m
	Electrical resistivity tomography	Internal	2D–3D	10^{-1}–10^{0} m
	Ground penetrating radar	Internal	2D	10^{-2}–10^{0} m
	Electro magnetic techniques	Internal	2D	10^{-2}–10^{0} m
	Micro¯gravimetry	Internal	1D	10^{-1}–10^{0} m
	Borehole loggings	Internal	1D	10^{-2}–10^{1} m
Others	Various field observations, already interpreted data	Surface	1D–2D	Variable

Internal: Information on the internal layer geometry.
[a] Surface: information on the landslide boundary at the ground surface.

Hummocky topography, bulges, depressions, cracks, slumps, bowed and deformed trees, and changes in vegetation are morphologic evidences of present and past landslide activity. In a complement to field recognition, these data can be extracted through the analysis of orthophotographs and high resolution DEMs (McKean and Roering, 2004; van Den Eeckhaut et al., 2005). Old documents (e.g. topographic maps, old photographs, cadastres) taken before the landslide event are very useful to localize main topographic and geometrical features covered by the landslide (e.g. crest, gully, berm). These geometrical features improve the interpretation of petro-physical and geotechnical data by localizing areas where physical contrasts are expected.

- *Geological data:* shear surface location can be interpreted from borehole logging, core photographs and observations in test pits or trenches for completing geological information at the ground surface. When geological maps are sufficiently detailed, two essential pieces of information can be used: the major geologic formations and the structural features (folds, joints, small faults, local shear zones and formation contacts; Sowers and Royster, 1978; Cornforth, 2005). The outcrops give information on the strength and stability of both intact and weathered materials that compose the landslide. They also allow one to identify the strongest formation susceptible to form the stable bedrock. Ground fissuring due to landslide movement has to be differentiated from fissuring attributed to other processes (e.g. human activity, soil desiccation, seismic events). Statistical analysis on changes in joint orientation, dip and azimuth in the landslide and in the surrounding area can be used to determine discontinuity families associated to the landslide and to the stable areas (Sowers and Royster, 1978; Jaboyedoff et al., 2009). In some cases, extrapolation of dip and azimuth of the observed interface (e.g. fractures, stratification planes) between the stable bedrock and the moving mass can be used as a first estimation of the landslide extension in depth.
- *Geotechnical data:* geotechnical data measured in boreholes (pressiometric tests, field vane shear tests) or from the ground surface (static or dynamic penetration tests) allow one to distinguish the weaker from the stronger formations (typically formation of the stable substratum) involved in the landslide. These data are direct measurements of the mechanical properties at different depth inside the moving mass. They complete the geological descriptions of the core and cuttings and constrain the petro-physical interpretations (Cornforth, 2005).
- *Petro-physical data:* petro-physical properties of the sub-surface (e.g., P- and S-waves velocity, electrical resistivity, dielectric permittivity, gravitational acceleration) measured at the ground surface or in boreholes (geophysical borehole logging, cross-holes measurements) provide a 2D or 3D imaging of the sub-surface (Jongmans and Garambois, 2007). Petro-physical properties are usually used to extent geotechnical and geological data determined with direct punctual in-situ measurements. Geophysical borehole logging systems (e.g. self-potential, electrical resistivity, nuclear radiation density based on nuclear absorption) provide very useful information when lateral correlation of geotechnical and geological data from adjacent boreholes are difficult due to strong variations of the soil properties or sampling gaps in the stratigraphic profile (typically core loss).

3. Method for multi-source data integration

Multi-source data have heterogeneous qualities and different spatial resolutions. Therefore data integration necessitates (1) to georeference the data in a common reference coordinate system, (2) to define their quality for the purpose of the modeling, and (3) to interpret (or re-interpret) the data to extract relevant information on the geometry. The proposed methodology is applicable to any kinds of digitized data. The main steps of the methodology are summarized in Fig. 1.

3.1. Georeferencing of data sources

Each source of data can be localized in different coordinate systems (2D, 3D) with variable accuracy thus making the georeferencing an important task (Kaufmann and Martin, 2008). Georeferencing processes available in Geographic Information System (GIS) softwares based on n-order polynomial transformations allow one to georeference digitized maps. The selected map projection has to be close to the digitized map for optimizing the alignment quality with a small number of control points. Otherwise, the map will be correctly aligned only in limited areas, independent of the number of control points. When more than three control points are available, the residual misfit between control point pairs can be used to estimate an error in horizontal location. Errors in georeferencing are often due to an insufficient quality or number of control points or to excessive distortions in the original maps (Caumon et al., 2009).

3D georeferencing of 2D rasterized cross-section is possible when at least two control points with the associated 3D coordinates in the reference coordinate system are known (e.g. geophysical sensors locations measured by GPS, benchmarks localized both in the cross-section and in a georeferenced map). Location of the control points in the reference coordinate system can be projected on a straight line calculated with a linear regression on the control points coordinate X–Y. The equation of the regression line is then used to compute the 3D position in the reference coordinate system of any location within the cross section.

The elevation data are often inaccurate or expressed as relative elevations. They can be corrected with a DEM used as elevation reference in the stable parts of the landslide. The elevation values inside the moving mass are obviously not considered because investigation can be acquired at several dates documenting different landslide morphology. The residual misfit between the reference DEM and the elevations in the stable part of the cross-section can be used to estimate an error in elevation.

3.2. Data quality evaluation: “hard” and “soft” data

The next step is to evaluate the quality of the data. The classification used in this work uses the concept of “hard data” and “soft data” initially defined by Poeter and Mckenna (1995) and Clarke (2004). “Hard data” are characterized by a high degree of reliability (e.g. explicit properties and very low uncertainties) while “soft data” are characterized by a low degree of reliability (e.g. implicit properties and higher uncertainties; Regli et al., 2004; Gallerini and De Donatis, 2009). The reliability index depends on (i) the quality of the original data source and (ii) the number of processing steps needed to extract useful information. The range of value for the reliability index is fixed on a scale between 1 (very soft) and 4 (very hard), and the criteria used for the categorization are defined as follows:

1. *Very soft data:* the original data are noisy, inaccurate for the purpose of the analysis and with a high degree of subjectivity in the interpretation. The original data do not have accurate spatial information. They are already in an interpretative format or are derived from inaccessible raw data.
2. *Soft data:* the original data need several steps of processing to extract a useful geometrical information. This is usually the case for indirect data such as petro-physical properties determined with geophysical techniques applied at the ground surface or in boreholes. The non-uniqueness of the inverted solution and the possible decreasing resolution with depth are some drawbacks affecting the accuracy of geophysical methods (Sharma, 1997; Jongmans and Garambois, 2007).
3. *Hard data:* the original data represents generally well the geometry of the landslide, even if some ambiguities in the interpretation still remain. The data have to be combined with other sources (generally

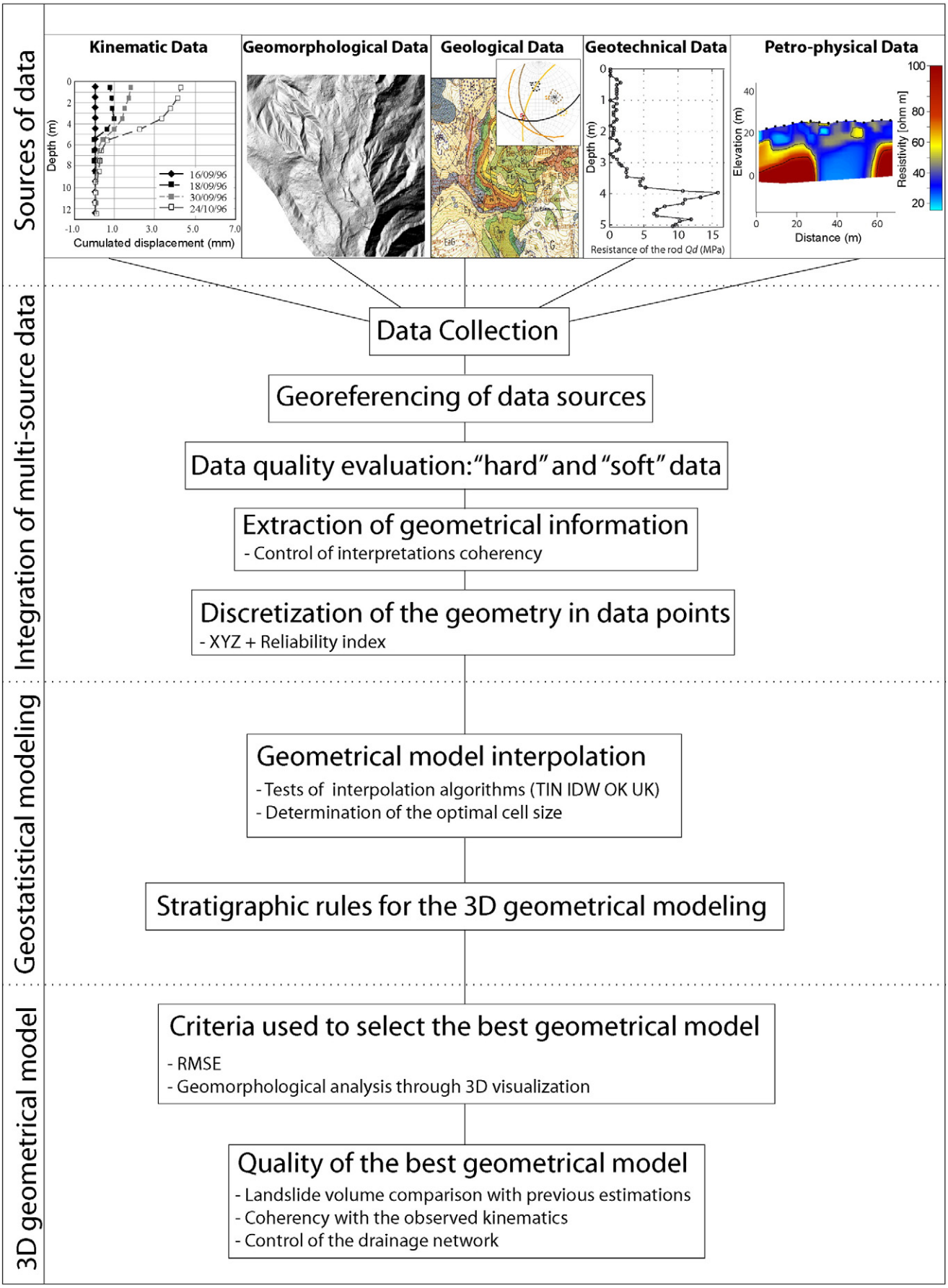

Fig. 1. Schematic workflow for multi-source data integration in a 3D geometrical model.

geotechnical tests and geological observations) to reduce the uncertainty in the interpretation.

4. *Very hard data:* the original data are sufficiently accurate and allow a straight-forward interpretation of the geometry without ambiguity. The data sources are generally direct geomorphological or geological observations, borehole cores and kinematic measurements.

Although this categorization is not objective and depends on the judgment of the interpreter, it has the advantage to be very flexible and adapted to a large amount of diverse data types.

3.3. Data (re-)interpretation: extraction of geometrical information

Hard data have to be used to constrain the interpretation of soft data. The main methods usually applied for identifying layering and discontinuities in geotechnical and petro-physical data are:

- The detection of sharp contrasts in petro-physical properties, reflecting transition between different layers and with the stable bedrock whose spatial extension can be mapped with imaging techniques (e.g. geophysical tomographies).
- The extrapolation of locally acquired hard data into spatially distributed acquisitions of soft data. The principle is to associate petro-physical or geotechnical parameters measured at the point scale to cross-sections of parameters measured with imaging techniques using empirical relations among the parameters or threshold values obtained from the literature or measured on soil samples.

3D visualization is absolutely necessary for an optimal interpretation of the data. An example of the main situations encountered for the interpretation of Electrical Resistivity Tomography (ERT) is detailed in Fig. 2. The interpretation of the resistivity profiles in Fig. 2A is very limited without the use of additional information located in the direct vicinity (Figure 2B.) By combining different analyses, the degree of freedom in the interpretation is reduced considerably. The interpretation of the internal structure becomes better constrained where stratigraphic and continuous petro-physical borehole logs are available (Sowers and Royster, 1978).

Possible spatial and temporal inconsistencies among interpretive data (cross-sections or stratigraphic logs) have to be controlled and

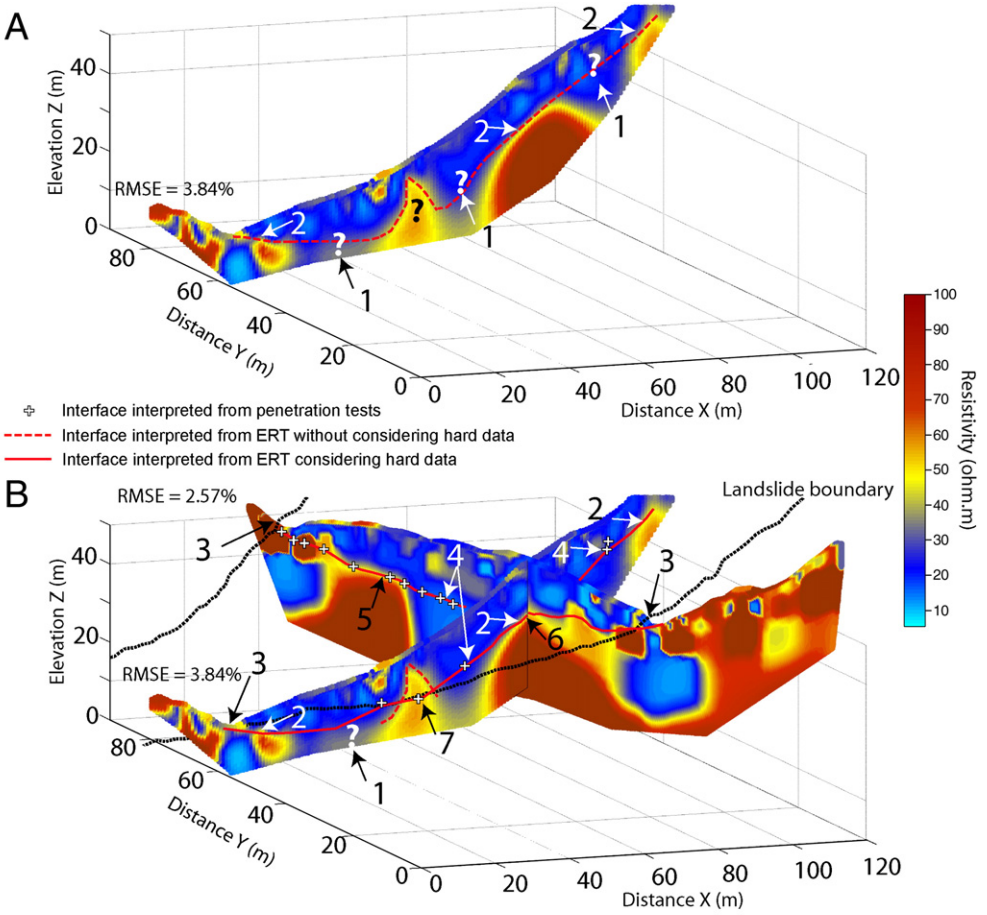

1. Example of area with a high degree of subjectivity in the interpretation
2. Identification of sharp properties contrasts
3. Contrast of resistivity value between the stable substratum (geomorphologic data) and the landslide area that can be observed in depth.
4. Interface extension with harder data (penetration tests)
5. Depth of resistivity contrast correlated with harder data (penetration tests) giving good confidence in the interpretation
6. Spatial coherency between cross-sections giving good confidence in the interpretation
7. Spatial incoherency with harder data (penetration tests). Priority is given to the hardest data.

Fig. 2. Example of interpretations of the Electrical Resistivity Tomography (ERT) data. A) Sharp property contrasts in the ERT allow to detect an interface in depth but the interpretation is limited without the use of additional information, B) Integration of all the information available close to the ERT profile displayed in 3D. The interpretation of the interfaces is more constrained. The normalized Root Mean Square Errors (RMSE) are also indicated.

corrected with hard data located in the vicinity of the acquisition using 3D visualization tools. For example, georeferenced maps draped in transparency on a shaded relief is a simple way to control the quality of the georeferenced maps (Caumon et al., 2009). The determination of the level above which inconsistencies become too important depends on the purpose of the geometrical model. If the purpose is to obtain an estimate of the volume of a landslide, a difference in depth determination of ca. 15% among two interpretations is acceptable, at the opposite, such an error can be too much important if the purpose of the model is to design remediation and reinforcement systems based on hydro-mechanical modeling.

Because of the possible non-unique solution of the inversion procedures, petro-physical cross-sections should be analyzed by constraining the inversion computation using a priori knowledge on the sub-surface geometry given by the more reliable interpretations available in the vicinity (Jongmans and Garambois, 2007). The introduction in the inversion procedure of the locations where sharp boundaries of petro-physical parameters are expected helps to considerably reduce the amount of possible solutions, thus leading to a greater consistency with the geological and geotechnical information (Lelièvre et al., 2008). Consequently a higher reliability index can be attributed to inverted models constrained by hard data. However, the petro-physical and geotechnical investigations are often done by different experts (geophysicians, geotechnicians) without a systematic exchange of information. Consequently a major task of the person in charge of the geometrical modeling is to use hard data to validate petro-physical inversions before incorporating them in the geometrical model.

Temporal inconsistencies (e.g. time-dependent geometrical changes) are more difficult to detect without repetitive data acquisitions and observations at the same location. In theory, the data should be acquired in a time short enough to avoid significant changes in the 3D geometry. In reality, these conditions are hardly ever realized because of temporal, financial and site configuration constraints. Therefore, recent data should have priority on older data. According to the quantity of available data, additional exploration in the field might be necessary.

3.4. Transformation of the information: discretization of the geometry

The extracted geometrical information is not directly useable as input for the 3D geometrical modeling. The different interfaces have to be discretized in data points (X,Y and Z) with a sufficient spatial density to preserve the main morphological details (Kienzle, 2004). This transformation is important as it controls the size of the mesh in the 3D geometrical model (Section 4.3.1).

A reliability index can be attributed to each data point (Section 3.2), and a confidence map can be associated to the geometrical model. This method allows one to set priority for the interpolation to the most reliable input data points. With this procedure, a null value for the reliability index is attributed for the areas unconstrained with data points.

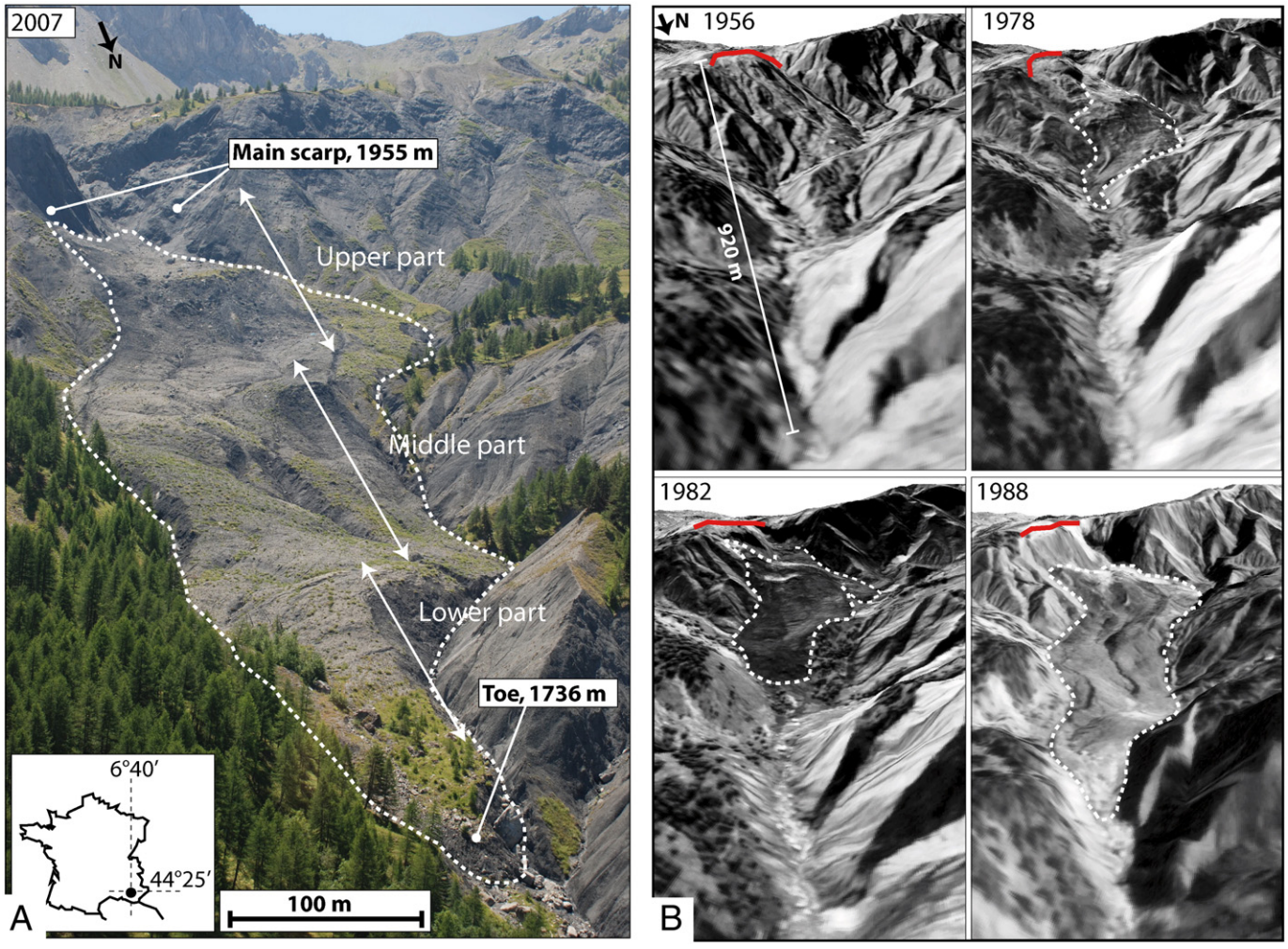

Fig. 3. General setting of the Super-Sauze mudslide. A) View of the mudslide from the North. B) Main evolution stages from the initial failure in the 1960's to the development of the mudslide tongue in 1988. The original torrential channel is progressively covered by the material (adapted from Weber and Herrmann, 2000).

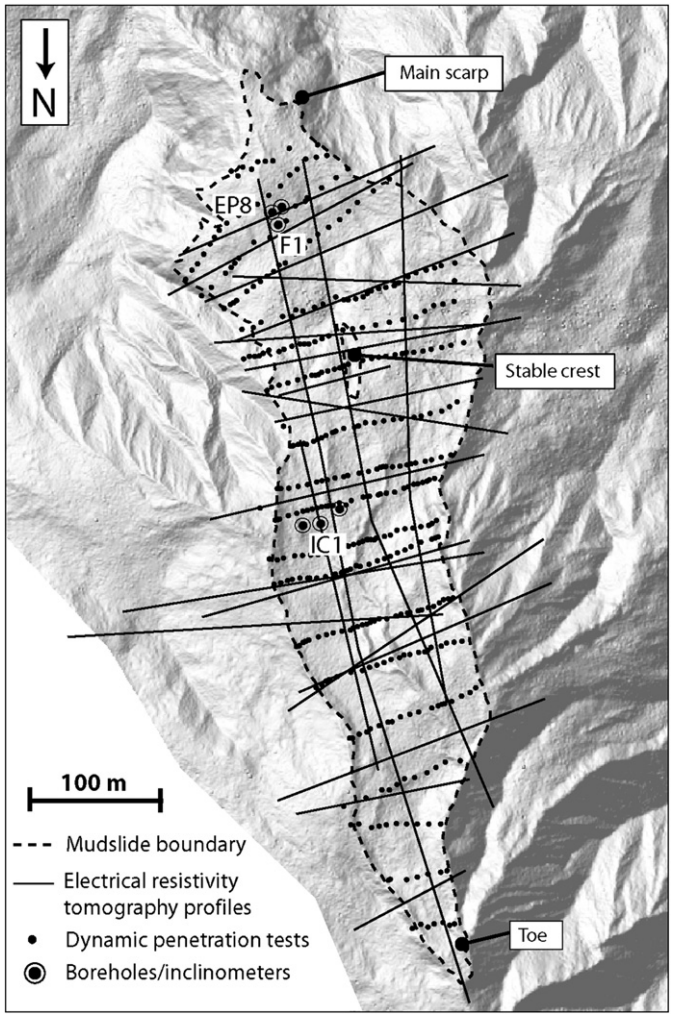

Fig. 4. Location of the geotechnical and geophysical investigations.

4. Application to the Super-Sauze mudslide

The methodology is applied to the Super-Sauze mudslide located in the Callovo-Oxfordian black marls of the Southern French Alps (Alpes-de-Haute-Provence, France). The landscape in which the mudslide has developed is characterized by a badland-type morphology (Figure 3A) with successions of crest and gullies.

Fig. 3B presents the main stages of development of the mudslide. Before the initial failure, the scarp area was affected by a deep seated slope deformation controlled by regional faults. In the 1960s, a succession of shallow plane and wedge failures occurred along some of the crests. The collapsed rocky panels progressively transformed into a silty sandy-matrix integrating marly fragments of heterogeneous sizes through weathering. In the late 1970s, the material started to accumulate downstream in the gullies. From the 1970s until today, the mudslide is gradually covering the talweg of the Sauze torrent with typical range of velocity between 1 to 3 cm d^{-1} and observed acceleration peaks until 40 cm d^{-1} in the spring season. In 2003, the total volume was evaluated at a maximum of 700,000 m^3 (Malet et al., 2003) based on a geotechnical investigation. In 2007, the mudslide extended over a distance of 920 m between an elevation of 2105 m at the crown and 1736 m at the toe with an average width of 135 m and a average slope of 25°.

Geomorphological, geological, geophysical and geotechnical investigations combined to a multi-parameter monitoring activity are conducted on the site since 1995. These investigations allowed a good identification of the main structures. Some attempts were realized to define the geometry of the landslide integrating the data acquired since then, essentially through 2D cross-sections (Flageollet et al., 2000; Malet, 2003). Starting in 1997, an important amount of geophysical prospecting (ERT, seismic, electro-magnetic; Schmutz et al., 2001; Méric et al., 2007; Grandjean et al., 2007; Schmutz et al., 2009) has been undertaken to extent spatially the information on the 3D geometry (Figure 4). However, some of the petro-physical data acquired during this period could not be integrated because of insufficient or inaccurate information on the positioning. Table 2 summarizes the data used for the 3D geometrical modeling as part of this work.

4.1. Characterization of the geometry and layering

The topography covered by the mudslide is composed of sub-parallel crests and gullies in the accumulation zone. Some of them emerge from the mudslide, whereas others are located a few meters below the ground surface. A three-layer structure with distinct mechanical properties has been proposed to characterize the internal structure. The identification of the layers is based on the information from dynamic penetration tests (395 dynamic penetration tests along 19 cross-sections; Figure 5), in-situ pressiometric and water injection tests, soil sampling and inclinometer measurements. A detailed description of the geomechanical and hydrological characteristics of the laters can be found in Flageollet et al. (2000) and Malet et al. (2003). The vertical layering of the mudslide can be summarized with:

- A surficial unit (C1) with a thickness ranging between 5 to 9 m (cone tip resistance Qd < 10 Mpa, pressiometric modulus E_M < 15 MPa). A

Table 2
Data available for the 3D geometrical modelling of the Super-Sauze mudslide.

Data type	Techniques	Quantity	Interfaces identified[a]		Date of acquisition	References
			C1–C2	C2(M)-S		
Kinematic	Inclinometers	3	X	X	1996	Malet, 2003
Geological	Borehole stratigraphic logs	5	X	X	1996	Malet, 2003
Geotechnical	Dynamic penetration tests	396	X	X	1996–2003	Flageollet et al., 2000; Malet, 2003
Geomorphologic	Field observations	–	Ground surface		2007–2009	–
	Aerial orthophotographs	7	Ground surface		1956*–1978*–1982*–1988* –1995*–2007**	*Weber and Herrmann (2000), **Sintegra company
	DEM (1 meter mesh, airborne lidar survey)	1	Ground surface		2007	Sintegra company
	DEM (15 meters mesh, aerial photogrammetry)	5	Ground surface		1956–1978–1982–1988 –1995	Weber and Herrmann (2000)
Petro-physical	2D electrical resistivity tomography	26	–	X	2004*–2005*–2006*–2008–2009	*Méric et al., 2007 ; *Grandjean et al., 2007
Others	Interpreted cross-sections	4	X	X	1996	Genet and Malet, 1997; Flageollet et al., 2000

Ground surface: landslide boundary at the surface.
[a] X: interface detected. The asterisk symbols link the dates of acquisition to the corresponding reference.

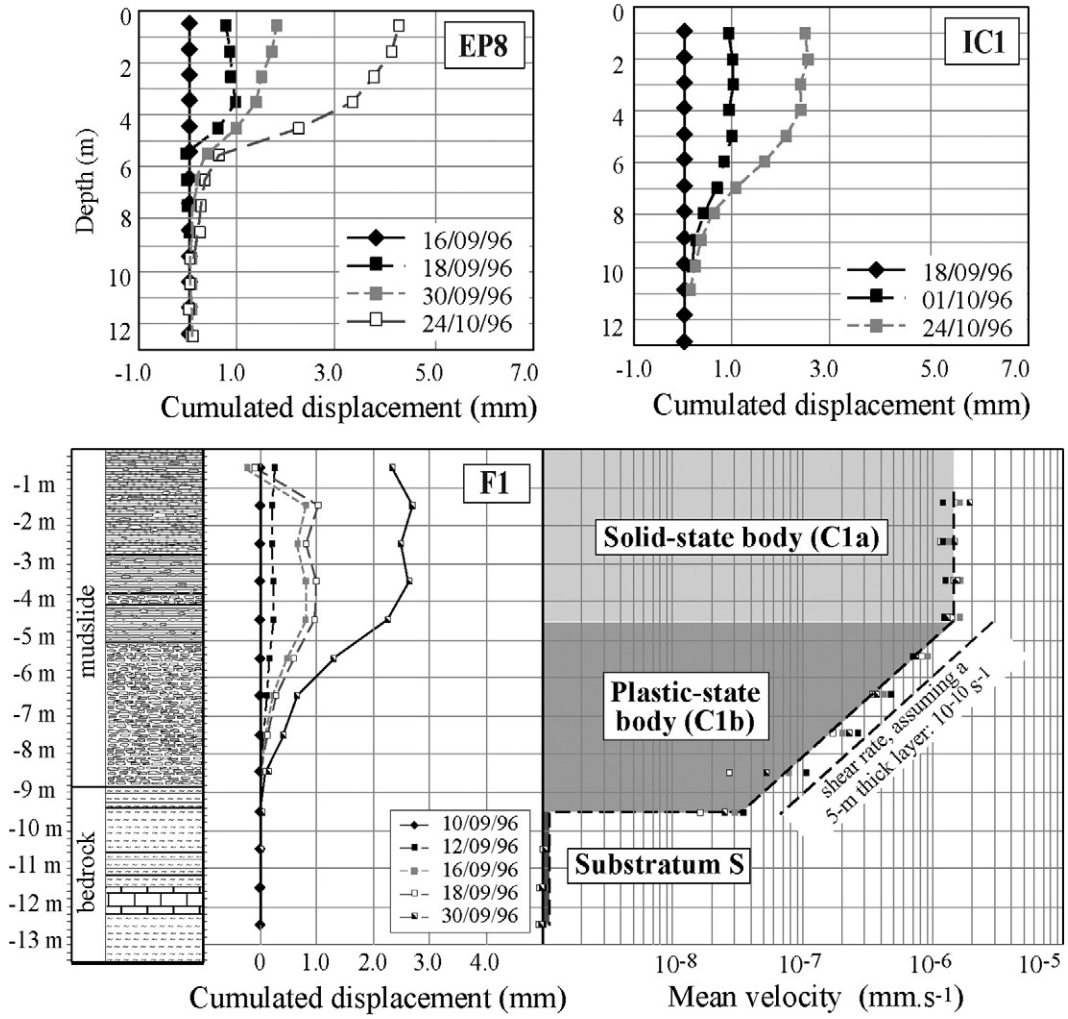

Fig. 5. Internal structure determined from inclinometer measurements and vertical profiles of displacement and velocity at three borehole locations. The borehole F1 is located at the vertical of an in-situ buried crest; at this position the layer C2 is not observed (Malet, 2003).

shear surface is identified at depths between 5 and 8 m. This unit is may be sub-divided in two secondary units for hydrogeological analysis; they are not distinguished in this study.

- A deep unit (C2) with a thickness ranging between 5 to 10 m. According to inclinometer measurements, pressiometric tests (E_M>15 MPa, pressure limit Pl>4 MPa) and water injection tests ($K<10^{-8}$ m s^{-1}), this unit is considered as very compact and impermeable. Inclinometer measurements showed that this unit is characterized by very low to even null displacement. It is associated to a "dead body" as observed at the Slumgullion earthflow (Varnes et al., 1996) and at the La Valette mudslide (Colas and Locat, 1993). In addition, the ancient torrent channel can be partially filled by significant thicknesses (several meters) of moraine deposits (M) before the occurrence of the landslide event (Weber and Herrmann, 2000).
- The stable substratum (S) composed of intact black marls (Qd>20 MPa).

26 ERT investigations were undertaken between 2004 and 2009 to spatially extend the punctual geotechnical and geological data (Schmutz et al., 2001; Grandjean et al., 2007; Méric et al., 2007) (Figure 6). Although the interface between C1 and C2 could not be detected, a significant contrast of resistivity can be observed between C2 (<~50 Ω m) and S (>~50 Ω m). The penetration test data (interpreted in terms of altitudinal position of the interface C2-S) located in at a distance of less than 5 m from the ERT lines are orthogonally projected on the profiles for validation (Figure 6):

- In the lower and middle parts of the mudslide, the C2-S interface interpreted from the penetration test data are in very good agreement with the C2-S interface interpreted from the ERT. This validates both the geophysical interpretations and the georeferencing of the ERT profiles. In addition, the correlation indicates that no significant change of the C2-S interface occurred between 1996 and 2008, thus reducing possible errors in the 3D geometrical model due to temporal inconsistencies.
- In the upper part of the mudslide, the correlation between the C2-S interface interpreted from ERT and from the penetration test data is more difficult to establish. Penetration tests were often affected by pseudo-blockages due to the higher frequency of blocks of moraine and panels of marls (Flageollet et al., 2000) limiting thus the investigation depth. In addition the sub-surface geometry seems more complex than in the middle and lower parts of the mudslide. Several crests observed in the orthophotograph of 1956 and buried by the mudslide are still present (Figure 7A).

Because the V-shape of the torrential valley is neither very well identified in the ERT profiles nor in the dynamic penetration tests in the middle part of the mudslide, ancient moraine formation and torrential deposits are highly suspected to have filled the torrent

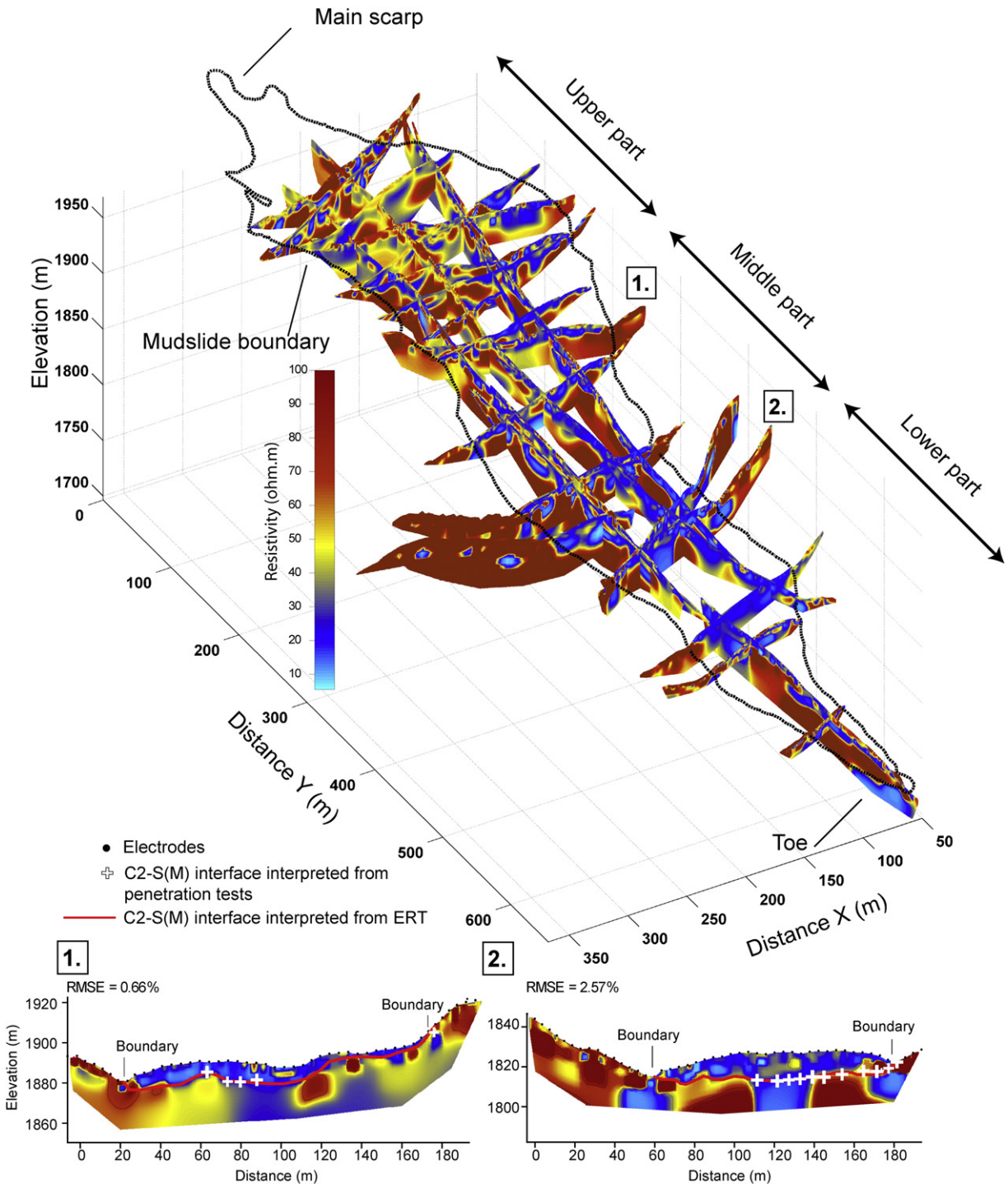

Fig. 6. Resistivity model of the mudslide. The Electrical Resistivity Tomography (ERT) profiles were acquired using Wenner and Wenner-Schlumberger arrays. The substratum depth identified is validated by projecting the information from the geotechnical penetration tests data on the ERT profiles. The normalized Root Mean Square Errors (RMSE) are also indicated.

valley in this area. The DEM of 1956 is therefore introduced in the 3D geometrical model to represent the contact between the moraine formation (M) and the substratum (S). The top of the moraine formation is called C2-(M)S, because in the other parts of the mudslide C2 is directly in contact with the substratum (S) without the presence of moraine. Therefore "(M)" means that intercalation of moraine deposit between C2 and S is possible. Similarly, the bottom of the moraine formation is called C2(M)-S. Where no moraine deposit is observed, the bottom of the mudslide is the contact C2-S.

4.2. Discretization of the geometry

As detailed in Section 3.3, the 3D coordinates of the data points are extracted from the georeferenced cross-sections and the landslide limits in such manner that the sub-surface topography is fully preserved. In addition, when a crest is identified both in the ERT data and on the orthophotograph of 1956, extra data points are added to constrain the interpolation of the 3D geometrical model (Figure 7A, B).

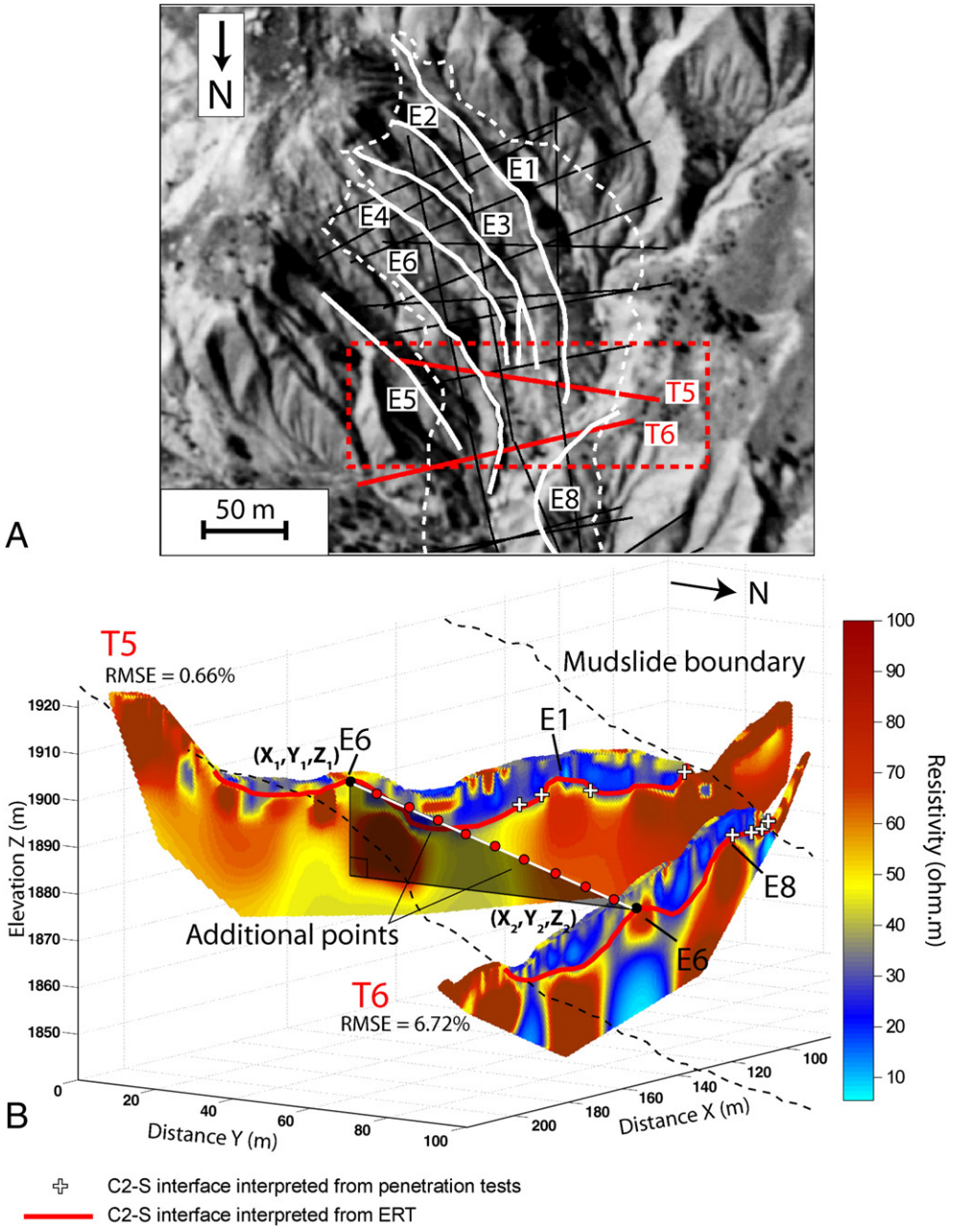

Fig. 7. Example of introduction of additional data points to constrain the 3D geometrical model. A) Main in-situ crests identified on an ortho-photography before the landslide event in 1956 and location of two Electrical Resistivity Tomography (ERT) profiles (T5, T6) crossing a series of crests. B) Detection of the in-situ crests in the resistivity model: the in-situ crest E6 is identified in the profiles T5 and T6. Extra data points are added along the profiles in order to integrate the spatial extent of the crests in the 3D geometrical model.

For the interface C1–C2, 1160 data points are available and are distributed mainly along profiles within a surface of 87.200 m^2. For the interface C2-(M)S, 3085 data points are available. In all cases, the mean sampling distance is about 3 m. Table 3 presents the reliability index attributed to each data point; the highest reliability index for each mesh of the model is presented in Fig. 8.

Table 3
Quantity and reliability index associated to the data points.

Data points	Kinematic	Geological	Geotechnical	Geomorphological (mudslide boundary)	Petro-physical	Already interpreted cross-section	Extra data points[a]	All data points
Interface unit	C1–C2							
Number of data points	3	–	336	726	–	95	–	1160
Reliability index	4	–	3	4	–	1	–	–
Interface unit	C2-(M)S							
Number of data points	3	5	336	726	955	95	965	3085
Reliability index	4	4	3	4	2	1	2	–

[a] Additional data points at the crest locations cf Fig. 7.

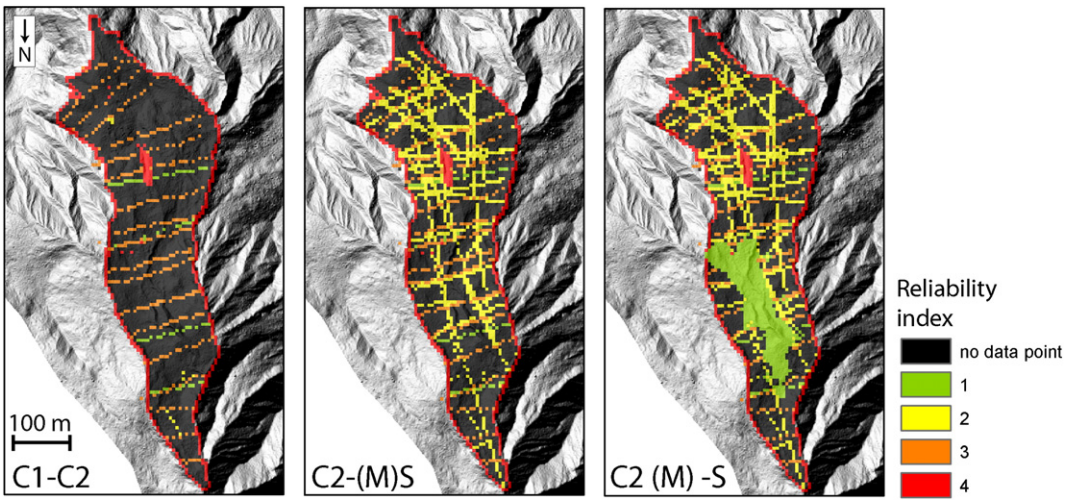

Fig. 8. Reliability index for the three interfaces. The area where the DEM of 1956 has been added is characterized with a reliability index of 1 (in green color).

4.3. Interpolation of the 3D geometrical model

The geostatistical modeling packages *RockWork©* (Rockworks, 2004) and *Surfer© v 8.01* (Golden software, 2002) were used to reconstruct the 3D geometrical model. The interactive graphical display window of *RockWork©* (*Rockplot3D*) is used for the 3D visualization. Among topographic interpolation algorithms, kriging yields usually better estimation of elevation than neighborhood approaches (Zimmerman et al., 1999) though these latter are sometimes more accurate (Declercq, 1996; Aguilar et al., 2005). These studies show that there is no fully objective rule for selecting an appropriate interpolation algorithm as it strongly depends on the characteristics of the surface being modeled, on the distribution of input data points and on data accuracy (Arnaud and Emery, 2000; Aguilar et al., 2005; Chaplot et al., 2006; Fisher and Tate,

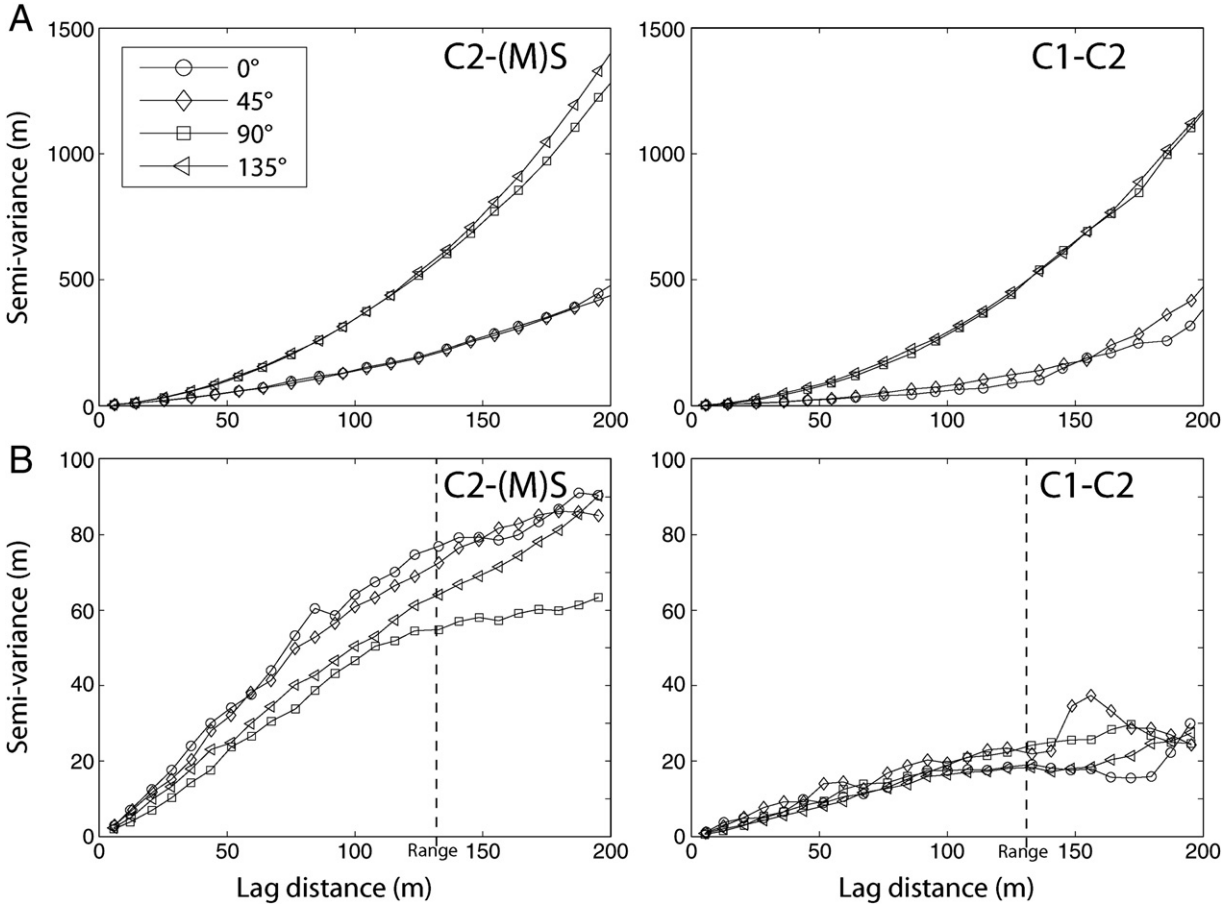

Fig. 9. Experimental semi-variograms of the input point data of the internal interfaces C2-(M)S and C1-C2. A) Semi-variograms used for Ordinary Kriging (OK) without detrend and with the application of a power law model without nugget; B) Semi-variograms of the residuals used for Universal Kriging after a planar detrend and the application of a linear model without nugget with a range of about 130 m.

2006; Kalenchuk et al., 2009). Furthermore, the creation of several geometrical models from the same set of input data (Caumon, 2010) and their further filtering through quality and validation methods (Maerten and Maerten, 2006; Moretti, 2008) is strongly recommended.

In this work, four interpolation algorithms commonly used in geomorphological researches are tested: Triangular Irregular Network (TIN; Jordan, 2006), Inverse Distance with a weighting factor n of 4 (IDW; Erdogan, 2009), Ordinary Kriging (OK; Zimmerman et al., 1999; Marinoni, 2003) and Universal Kriging (UK; Zimmerman et al., 1999; Gundogdu and Guney, 2007).

TIN uses an optimal and fast Delaunay triangulation procedure in order to satisfy the requirement that a circle drawn through the three nodes of a triangle will contain no other node (Lee and Schachter, 1980). IDW estimates elevations at unknown location using the distance and values to nearby known data points, based on the assumption that each data point influences the resulting surface up to a finite distance (Chaplot et al., 2006). The weight given to the influence of nearby known data point is inversely proportional to a power ($n=4$) of the distance. Kriging interpolation techniques take into account the stochastic dependence among data points (which may be the result of a geological process such as sedimentation; Burgess et al., 1981; Marinoni, 2003). OK is the simplest algorithm of kriging in which the input elevation data are assumed to be stationary, without any drift. UK is a variant of OK and is applied where input data points contain a local trend. A structural analysis of the spatial correlation (e.g. semi-variograms) among the input data points carried out before the interpolation (Marinoni, 2003). The TIN and IDW grids are computed in *RockWork©*; the OK and UK grids are computed in *Surfer©*.

4.3.1. Analysis of the spatial structure of the data points

The structure of the input data points of the interfaces C1–C2 and C2-(M)S is assessed using semi-variograms for the directions 0°, 45°, 90° and 135° relative to the sliding direction of the mudslide (Figure 9A, B). Fig. 9A shows the experimental semi-variograms introduced in OK for both interfaces. An important spatial structure and a marked anisotropy due to the terrain slope are observed. The unbounded semi-variograms (no range) indicate non-stationary data that can be modeled with a power semi-variogram without nugget. Because of the presence of a trend in the data points caused by the terrain slope, UK interpolation may be more accurate (Royle et al., 1981). After removing the trend with a planar regression, the semi-variograms are computed on the residual between the trend and the elevation values of the data points (Figure 9B). The experimental semi-variograms can be modeled with a linear relationship without nugget with a range of about 130 m. The presence of a range (distance at which elevation data become uncorrelated) indicates that the data stationarity assumption is respected (Bancroft and Hobbs, 1986).

4.3.2. Determination of the optimal cell size of the geometrical model

Different methods are available to determine the optimal grid resolution (Hengl, 2006). In this work, the choice of the resolution is based on the Nyquist-Shannon sampling theorem for signal processing (Shannon, 1949) which states that a continuous function can be fully reproduced if sampling frequency is two times the original frequency. From a geomorphological point of view, the mesh size should at least correspond to the average spacing between inflection points of the terrain (e.g. locations where the curvature or the slope of the terrain changes sign). The principle is explained in detail in Hengl (2006). In this work, the problem is simplified in one dimension with the following relationship (Eq. (1)):

$$r \leq \frac{1}{2n}\sum_{i=1}^{n} \Delta x_i \quad (1)$$

where r is the maximal theoretical mesh size and n is the number of Δx (distance between two inflection points).

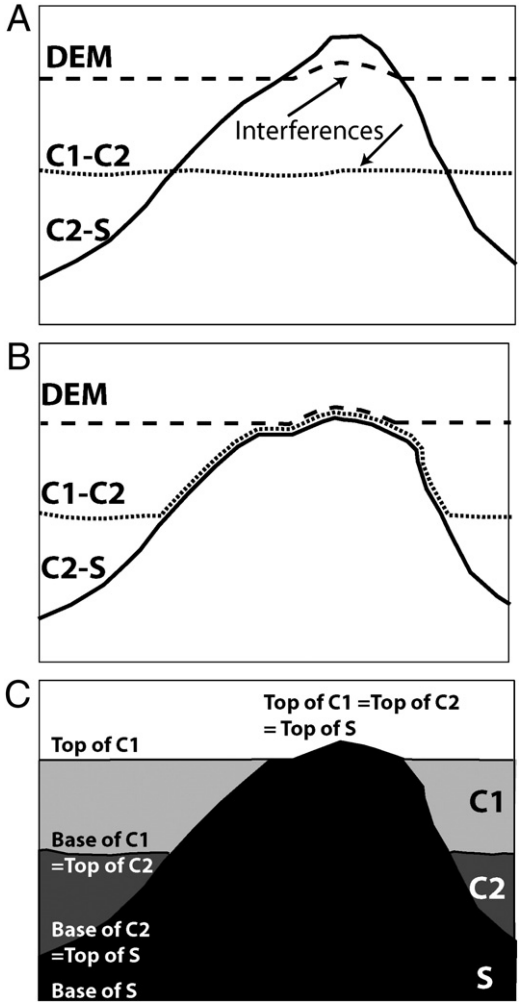

Fig. 10. 3D stratigraphic rules used for the interpolation in *Surfer* to avoid interferences among the internal layers. A) Interferences of the C1–C2 interface with the C2-S interface. B) Application of the stratigraphic rules. In order to stop the C1–C2 interface, the elevation values are set equal to those of the C2-S interface. The same method is applied for all the interfaces crossing the ground topography; C) Output representation of the interfaces for the 3D visualization in *Rockplot3D*.

Data points extracted from the interpretation of continuous imaging (e.g. ERT) or dense geotechnical investigation along profiles showing major variations in elevation are used to define the cell size. A n-order polynomial continuous function is fitted on the data point to model the sub-surface topography interpreted in each cross-section. The sub-surface inflection points are then automatically localized for each position where the first and second derivatives of the function equal to zero.

Because the determination of r is computed along transversal cross-sections, r does not take into account the density and the spatial distribution of the data points which are important parameters in the choice of the cell size (Bishop and McBratney, 2001; Aguilar et al., 2005; Fisher and Tate, 2006). If the cell size is too small, artificial surface roughness can be created in areas insufficiently constraint by the data points (Bishop and McBratney, 2001; Hengl, 2006). Therefore the influence of the cell size r on the geometrical model has to be controlled by 3D visualization.

In the case of the Super-Sauze mudslide, the C2-(M)S interface in the transversal ERT profiles (Figure 6) is used to determine the cell size because this interface presents the greatest variations in elevation. For a better representation of the sub-surface morphological features, the median value of the distance between crests and gullies (10.2 m) determined in the cross-sections is chosen; it

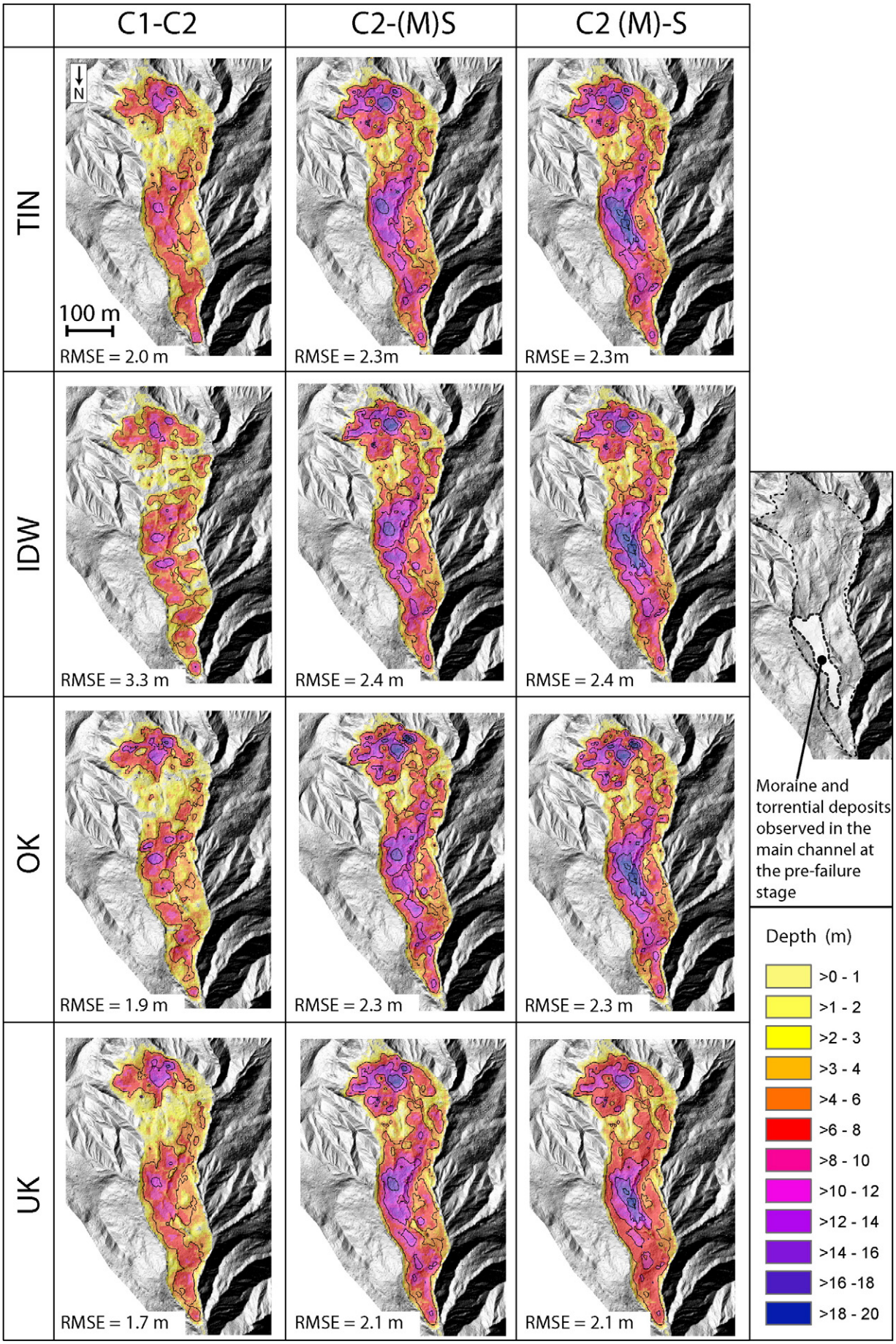
C1-C2
C2-(M)S
C2 (M)-S
TIN
IDW
OK
UK
N
100 m
RMSE = 2.0 m
RMSE = 2.3m
RMSE = 2.3m
RMSE = 3.3 m
RMSE = 2.4 m
RMSE = 2.4 m
RMSE = 1.9 m
RMSE = 2.3 m
RMSE = 2.3 m
RMSE = 1.7 m
RMSE = 2.1 m
RMSE = 2.1 m
Moraine and torrential deposits observed in the main channel at the pre-failure stage
Depth (m)
>0 - 1
>1 - 2
>2 - 3
>3 - 4
>4 - 6
>6 - 8
>8 - 10
>10 - 12
>12 - 14
>14 - 16
>16 -18
>18 - 20

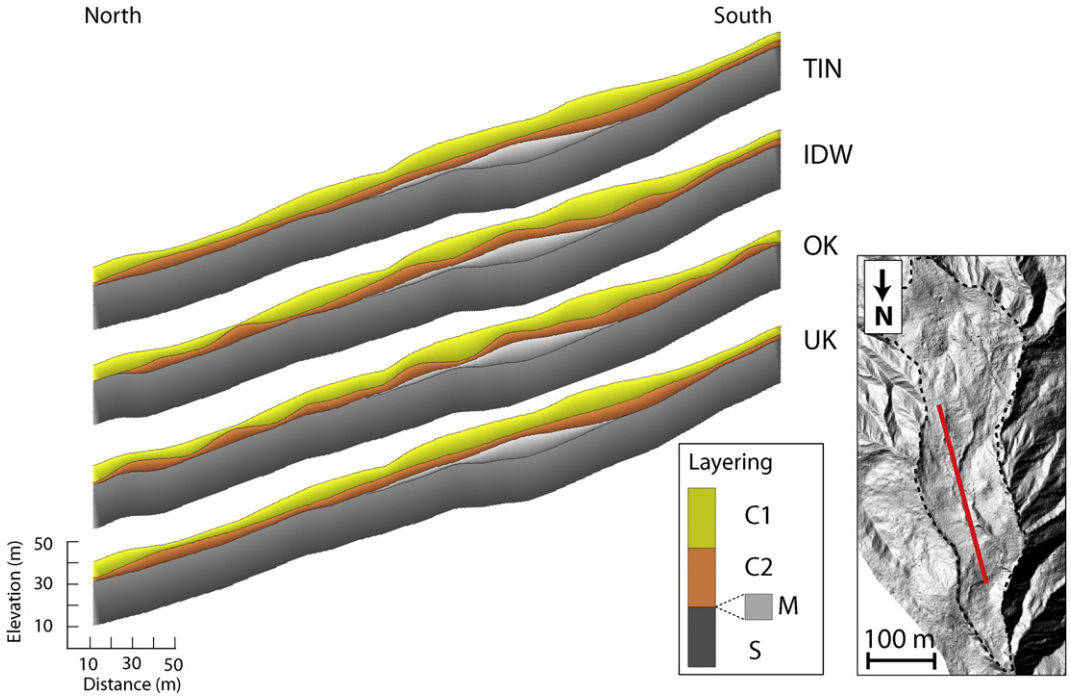

Fig. 12. Analysis of the 3D geometrical model through visualization. Cross-sections in the 3D geometrical models pointing out the undulating C1–C2 interface produced by IDW and OK (see Figure 11 for the acronyms of the interpolation algorithms). The location of the cross-section is also indicated.

corresponds to a maximal grid resolution of about 5 m. Because the mean spacing between the transversal cross-sections in the North direction is about 23 m, the grid resolution of 5 m is not refined.

4.3.3. Stratigraphic rules for the 3D geometrical modelling

Each unit within the landslide is delimited by a top and a base interface that have to be compliant with the data points. However to obtain a geometrical model in agreement with the geological information, this condition is not sufficient, and stratigraphic rules are defined to avoid interferences between interfaces (Mallet, 2004; Caumon et al., 2009; Figure 10). In the case of the Super-Sauze mudslide, the following rules are applied:

- The layer interfaces cannot rise above the ground topography;
- The top interface and the base interface of an internal unit cannot intersect each other;
- The internal units within the landslide cannot cross the stable substratum.

These rules are automatically managed by the 3D stratigraphic module of *RockWork*© by setting a relative stratigraphic chronology to each unit of the model. This is not the case in *Surfer*© where each interface is interpolated individually. Therefore a post-processing is necessary on the surfaces created with *Surfer*© to correct the incoherencies as is illustrated in Fig. 10. A moving average filter is applied on the gridded surfaces to reduce the influences of small-scale variability between neighboring data points. Finally, the output of each unit is expressed in a top and a base interface for 3D visualization in *Rockplot3D*.

4.3.4. Criteria used to select the best geometrical model

The accuracy of gridded surfaces can be evaluated through quantitative and qualitative indicators; in this work the model has to satisfy two conditions:

- The gridded surface should present a low value of Root Mean Square Error (RMSE; Erdogan, 2009; Eq. 2):

$$RMSE = \sqrt{\frac{1}{n}\sum_{i=1}^{n}\left(Z_i^{model} - Z_i^{true}\right)^2} \quad (2)$$

where n is the total number of data points, Z^{model} is the elevation predicted by the model and Z^{true} is the elevation of the withheld data set.

In order to compute the RMSE, a subset of data points with a high degree of reliability is withheld from the interpolation by applying a random split-sample method (Declercq, 1996). A sample of sixty dynamic penetration tests data (of both interfaces) is therefore not introduced in the interpolation.

- The gridded surface does not have to present strongly undulated features and local depressions or abrupt elevation changes. The historical development of the mudslide provides information on the sequence of organization of the layers (Figure 3B). Since the mudslide is progressively burying an ancient torrential stream, a layering approximately parallel to the slope gradient is expected rather than a strongly undulated geometry which is often an artefact of the interpolation (Malet, 2003). 3D visualization is used to determine the location of unrealistic morphological features (Aguilar et al., 2005; Fisher and Tate, 2006).

4.4. Results of the 3D geometrical modeling

4.4.1. Identification of the best geometrical model

Fig. 11 presents the thickness maps (e.g. depth with reference to the ground surface) of all gridded interfaces and the respective RMSE value. A small range of RMSE values (1.7 to 3.3 m) is calculated. The UK algorithm presents the lowest values. However the RMSE is not

Fig. 11. Maps of the internal interface C2-S interpolated with different algorithms (TIN: Triangular Irregular Network; IDW: Inverse Distance; OK: Ordinary Kriging; UK: Universal Kriging) with a mesh grid of 5 m. The depth relative to the ground surface given by the airborne LiDAR DEM is presented. The location where moraine and torrential deposits are observed between the layers C2 and S is also indicated.

sufficient to evaluate the quality of the geometrical models because it depends on the spatial distribution of the subset of data used for the calculation. Furthermore, the RMSE is based on the assumption that errors are random and normally distributed around the true value which is not always guaranteed (Desmet, 1997). Therefore qualitative comparison through visualization is also used to evaluate the quality.

The 3D visualization of the different surfaces indicates that IDW and OK tend to produce undulated interfaces in areas unconstrained by data points (Figure 12); TIN and UK provide more regular geometries. As no strong undulations are observed in the C2-(M)S interface with the UK interpolation method and because it presents the lowest RMSE, these gridded surfaces are considered as the more suitable (Figure 13). Table 4 presents the statistics of thickness for each layer with an estimation of the associated volumes.

4.4.2. Quality of the best geometrical model

The quality evaluation of geological reservoirs (e.g. water, gas, oil) is systematically evaluated by quantitative approaches such as line and surface balancing or gravity modeling (Martelet et al., 2004; Moretti, 2008). In this work, the quality control of the selected geometrical model is based on (i) the comparison of computed volumes with previous estimations, (ii) the coherence among the model geometry and the observed kinematics of the landslide, and (iii) the reliability of the location of the drainage networks (Chaplot et al., 2006).

(i) The volume of the mudslide estimated with the 3D geometrical model is of ca. 560,000 m^3 which is in the range of the first approximation of about 700,000 m^3 based on 2D cross-section analysis (Malet et al., 2003; Table 4). About 66% of the total volume corresponds to the most active unit C1.

(ii) The global trend of the geometry is particularly well reproduced in the vicinity of the emerged crest E3 and of the buried crest E8 which control part of the deformation mechanism (Figure 13; Flageollet et al., 2000; Malet et al., 2002). In the upper part of the mudslide, the moving-mass material is deviated by the crest E3 in two parts. On the Western part of E3, the material is transported in a large channel of ca. 6 m deep and 30 m in width. In this channel, high displacement rates (several centimeters per day) are observed because of the concentration of water fluxes and the development of high pore water pressures. In the middle part of the mudslide, the crest E8 is an obstacle to the transport of material downstream;

Table 4
Estimated thickness and volume of the internal layers.

	Mean (m)	Standard deviation (m)	Min (m)	Max (m)	Volume (m^3)
C1	5.4	2.6	0.0	16.4	374,800
C2	3.3	1.8	0.0	9.8	185,600
Total mudslide	7.5	3.6	0.0	19.9	560,400
Moraine deposits M (in the main channel at the pre-failure stage)	3.4	3.0	0.0	8.0	35,600

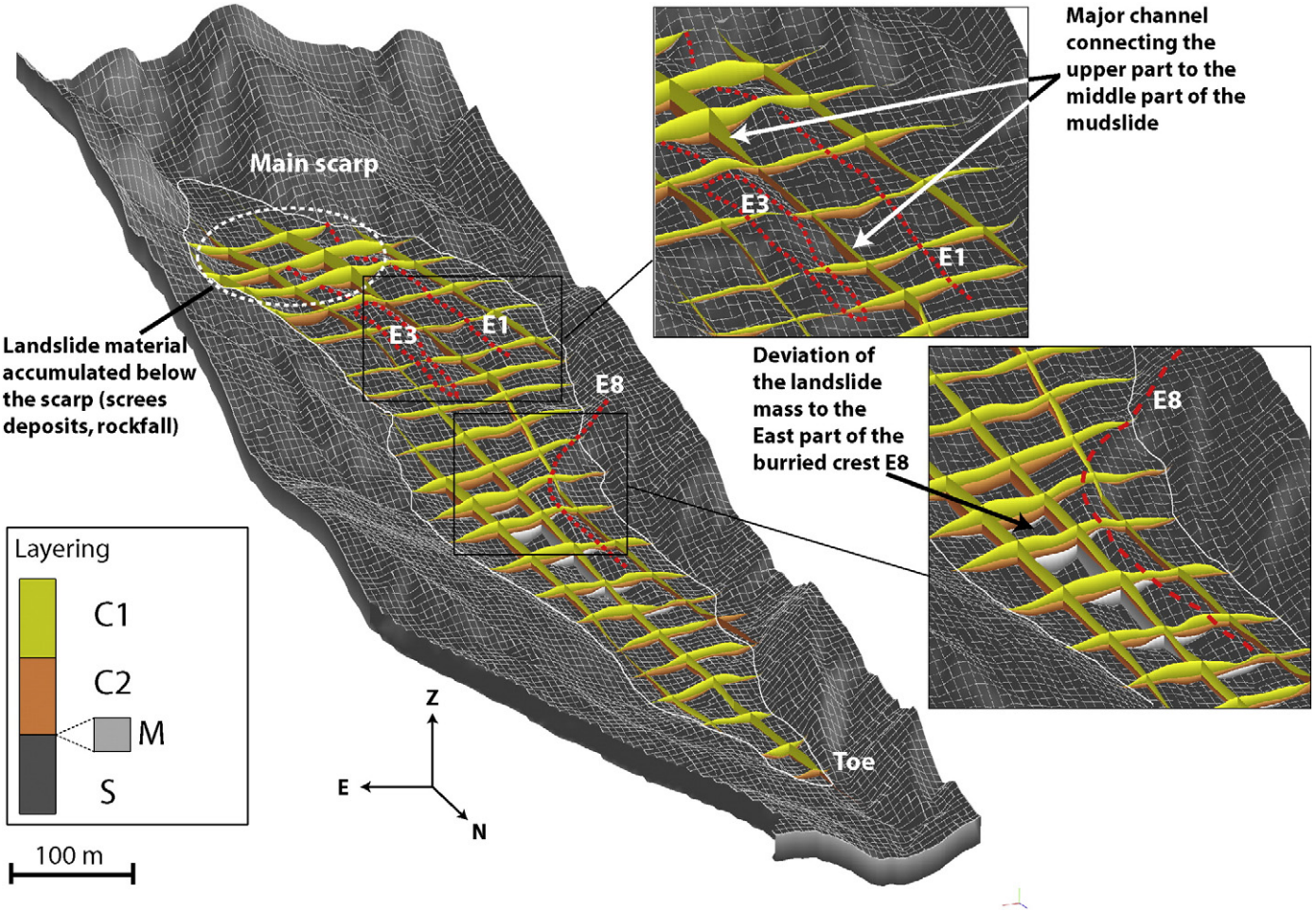

Fig. 13. 3D geometrical model of the Super Sauze mudslide interpolated with Universal Kriging (UK) and illustrated through stratigraphic cross-sections. The geometry of the most important crests controlling the dynamic of the mudslide (emerged crest E3, buried crests E1 and E8) is well reproduced.

consequently, the material accumulate on the Eastern part of E8 where the highest thickness (ca. 20 m) is observed.

(iii) The position of the drainage networks in the gridded surfaces of the C2(M)-S interface is in agreement with the position observed on the photogrammetric DEM of 1956 and the ortho-photographs of 1956 before the failure (Figure 14; Weber and Herrmann, 2000).

5. Discussion

The proposed methodology illustrates that many steps are necessary to construct sound and reliable landslide 3D geometrical models by integrating highly heterogeneous multi-source data. For the Super-Sauze mudslide, the data were irregularly distributed along profiles. Such data point distributions are common in the case of petro-physical investigation techniques. In order to evaluate the sensitivity of the 3D geometrical model to data point spacing, some data points of the interface C2-S(M) were not introduced to obtain a more spatially homogenous (4.10^{-3} pts m^{-2}) but less dense distribution (Figure 15). UK was applied to interpolate a new C2-S(M) interface that is compared with the C2-S(M) interface interpolated by introducing all the available data points. The main differences are obviously located in the upper part of the mudslide where the topography is the most complex. The crest locations in this area cannot be correctly modeled because the sub-surface topography is undersampled. In the middle and the lower parts of the mudslide, the differences are less important because the sub-surface topography is simpler. However, without an a priori conceptual model, it is difficult to determine the optimal spatial distribution of measurements and define an investigation planning without the risk of undersampling significant sub-surface features.

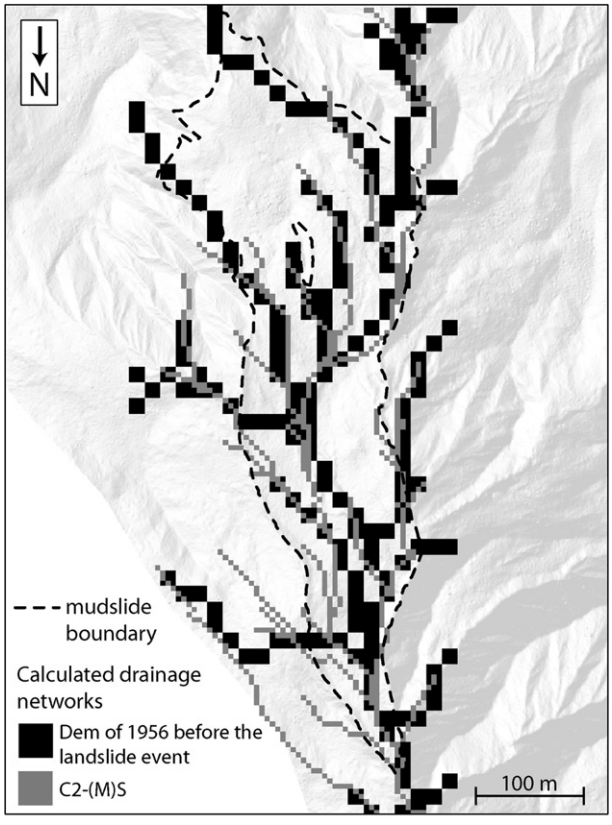

Fig. 14. Comparison of the location of the drainage networks identified on the interpolated C2-(M)S interface and on the interpretation of the 1956 ortho-photograph and DEM.

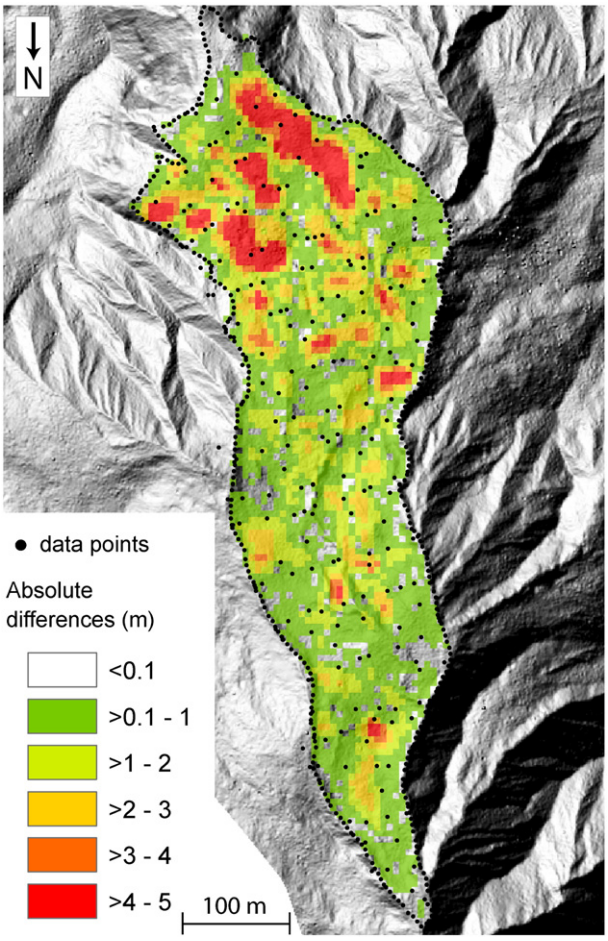

Fig. 15. Absolute difference between the C2(M)-S interface and a the interpolated C2(M)-S interface (Universal Kriging algorithm) with homogenously distributed input data points.

Spatially distributed techniques like geophysics are very efficient for preliminary field investigations because they can provide a continuous imaging of the subsurface. However, the tomographies produced by geophysical inversion generally display a smooth image of the sub-surface. The sharp geometry of the crests can hardly be reproduced. An example is detailed in Fig. 16. A cross-section obtained from the gridded surfaces is compared with an "expert" cross-section generated using the same input data (Flageollet et al., 2000). The right part of the cross-sections of the model is consistent with the "expert" interpretation. However, the left part is not constrained by data located on the profile and the gridded surfaces are interpolated from adjacent ERT profiles. The sub-surface appears excessively smoothed compared to the reality. In such conditions or if no data are available in a specific area, it is necessary to force the model to produce realistic results by adding data points coming from expert knowledge. A lower reliability index of the gridded surface has however to be attributed in this case.

The dynamics of a mudslide can significantly affect the accuracy of the geometrical model when sub-surface exploration is planned over long periods. In the case of the Super-Sauze mudslide, the position and the local geometry of the interface between the nearly stable layer C2 ("dead body") and the stable substratum are not varying over the period 1996–2009 (Section 4.1). However this statement cannot be ensured for the interface C1–C2 investigated over the period 1996–1999 through geotechnical investigation. In contrast to landslides that behave as more or less rigid bodies, mudslides can display complex deformation pattern similar to those of viscous fluids. In periods of

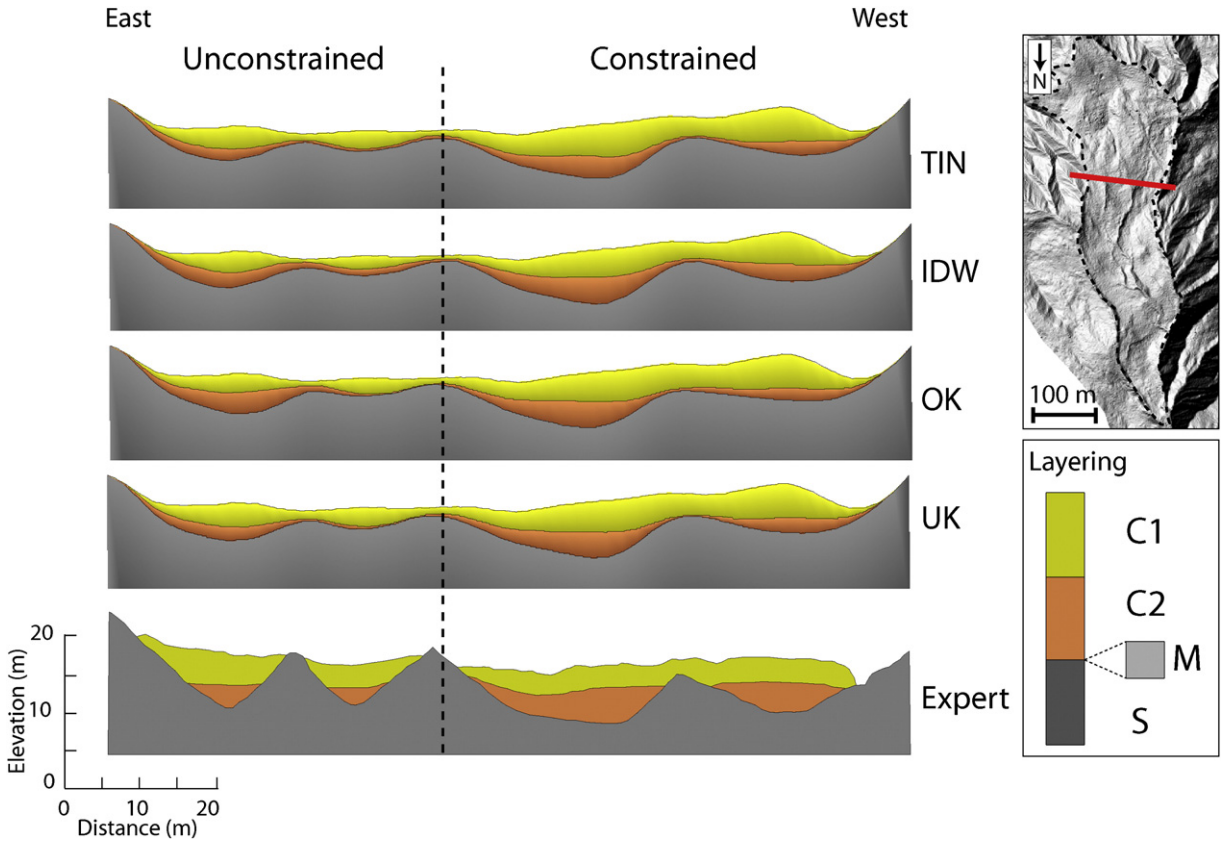

Fig. 16. Comparisons of cross-sections extracted from the 3D geometrical model (TIN, IDW, OK and UK interpolation algorithms) with a reference ground topography of 2007, and an "expert" cross-section interpretation with the ground topography of 1996 (adapted from Flageollet et al., 2000). The Western side of the cross-sections is well constrained by the input data points while the Eastern side is not constrained. The location of the cross-section is also indicated.

high displacement rates, the deformation of the entire layer C1 can be predominant to the deformation concentrated at shear zones in depth (Picarelli et al., 2005). Therefore it is likely that the position and the local geometry of the interface C1–C2 can change in time. It is worth mentioning that a more accurate geometrical model would require additional field investigation at very high resolution at shallow depths to better identify the location of this interface.

6. Conclusion

A methodology to extract useful information on the geometry and layering of landslides from heterogeneous data sources and to integrate the information in a 3D geometrical model is presented. Data georeferencing and re-interpretation are the most important steps in the workflow. Although these processing steps are relatively simple in theory, they are absolutely necessary to detect inconsistencies among multi-source data. A simple approach is proposed to evaluate the quality of the data through a reliability index. The Nyquist-Shannon theory is used to determine the optimal cell size for the interpolation of the gridded surface from the original data points. Using simple stratigraphic rules, 3D modeling based on 2D gridding processes is sufficient to model the geometry of landslides characterized by continuous and sub-parallel layering.

The methodology is applied to the Super-Sauze mudslide for which an extensive dataset of geophysical, geotechnical and geomorphological observations is available. The 3D geometrical model allows one to estimate the volume of the moving mass to 560,000 m^3. Several controls of quality have been carried out in order to ensure that the 3D geometrical model is suitable for further detailed hydro-mechanical modeling. The information on the sub-surface geometry is derived mostly from indirect data (ERT) which provide a relatively smooth imaging of the sub-surface combined to direct data coming from geotechnical tests.

A future challenge to improve the proposed methodology relies on coupling of 3D Geographic Information Systems (data storage and management) with 3D geometrical modeling packages (Apel, 2006; Kaufmann and Martin, 2008; Jones et al., 2009). The data can be structured and stored according to their major characteristics (e.g. nature, reliability index, date of acquisition, positioning) allowing a quick re-interpretation and an easier upgrading of the 3D geometrical model. Depending on the quantity of data available, the development of 4D geometrical models (with time) would then be possible. However, quality control remains absolutely necessary. For example, volume balancing can be a way to control the quality of the geometrical models by comparing the total amount of material failed in the ablation zone to the volume of material stored in the accumulation zone (considering a swelling factor due to the increase of porosity of the mobilized material). The development of statistical methods to better quantify the uncertainty of the geometrical models is also necessary.

Acknowledgements

This work was supported by the European Commission under the Marie Curie Contract '*Mountain Risks: from prediction to management and governance*' (MCRTN-035798). All reference and monitoring data are freely available on the OMIV (French Observatory of Landslides) website: http://eost.u-strasbg.fr/omiv/. The authors would like to acknowledge Julien Ponton (University of Strasbourg) for his support to the acquisition of the electrical resistivity tomography in the field. The authors are also grateful to Peter Bobrowsky and Thom Bogaard for their suggestions which were very helpful to improve the manuscript.

References

Aguilar, F.J., Agüera, F., Aguilar, M.A., Carvajal, F., 2005. Effects of terrain morphology, sampling density and interpolation methods on grid DEM accuracy. Photogrammetric Engineering & Remote Sensing 71 (7), 805–816.

Angeli, M.C., Pasuto, A., Silvano, S., 2000. A critical review of landslide monitoring experiences. Engineering Geology 55, 133–147.

Apel, M., 2006. From 3D geomodelling systems towards 3D geoscience information systems: data model, query functionality and data management. Computer & Geosciences 32, 222–229.

Arnaud, M., Emery, X., 2000. In: Hermès (Ed.), Estimation et interpolation spatiale : méthodes déterministes et méthodes géostatistiques. 216 pp.

Bancroft, B.A., Hobbs, G.R., 1986. Distribution of kriging error and stationarity of the variogram in a coal property. Mathematical Geology 18 (7), 635–652.

Bichler, A., Bobrowsky, P., Best, M., Douma, M., Hunter, J., Calvert, T., Bunrs, R., 2004. Three-dimensional mapping of a landslide using a multi-geophysical approach: the Quesnel Forks landslide. Landslides 1 (1), 29–40.

Bishop, T., McBratney, A., 2001. A comparison of prediction methods for the creation of field-extent soil property maps. Geoderma 103 (1–2), 149–160.

Brunsden, D., 1999. Some geomorphological considerations for the future development of landslides models. Geomorphology 30, 13–24.

Burgess, T.M., Webster, R., McBratney, A.B., 1981. Optimal interpolation and isarithmetic mapping of soil properties: sampling strategy. Journal of Soil Science 32, 643–659.

Casson, B., Delacourt, C., Baratoux, D., Allemand, P., 2003. Seventeen years of the La Clapière landslide evolution analysed from ortho-rectified aerial photographs. Engineering Geology 68, 123–139.

Caumon, G., Collon-Drouaillet, P., Carlier, Le, de Veslud, C., Sausse, J., Visuer, S., 2009. Teacher's aide: 3D modeling of geological structures. Mathematical Geosciences 41 (9), 927–945.

Caumon, G., 2010. Towards stochastic time-varying geological modeling. Mathematical Geosciences 42, 555–569.

Chaplot, V., Darboux, F., Bourennane, H., Leguédois, S., Silvera, N., Phachomphon, K., 2006. Accuracy of interpolation techniques for the derivation of digital elevation models in relation to landform types and data density. Geomorphology 77, 126–141.

Clarke, S.M., 2004. Confidence in geological interpretation. A methodology for evaluating uncertainty in common two and three-dimensional representations of sub-surface geology. British Geological Survey Internal Report, IR/04/164. 29 pp.

Colas, G., Locat, J., 1993. Glissement et coulée de La Valette dans les Alpes-de-Haute-Provence: présentation générale et modélisation de la coulée. Bulletin de Liaison du Laboratoire des Ponts et Chaussées 187, 19–28.

Cornforth, D.H., 2005. Landslides in practice: investigation, analysis and remedial/preventative options in soils. Wiley, USA. 624 pp.

Crozier, M.J., 2010. Landslide geomorphology: an argument for recognition, with examples from New Zealand. Geomorphology 120 (1–2), 3–15.

Cruden, D.M., Varnes, D.J., 1996. Landslide types and processes. In: Turner, A.K., Schuster, R.L. (Eds.), Landslides-investigations and mitigation. : Transportation Research, 247. National Academy of Sciences, Washington D.C, pp. 36–75. Board Special Report.

Delacourt, C., Allemand, P., Berthier, E., Raucoules, D., Casson, B., Grandjean, P., Pambrun, C., Varel, E., 2007. Remote-sensing techniques for analysing landslide kinematics: a review. Bulletin de Société Géologique de France 178 (2), 89–100.

Declercq, F., 1996. Interpolation methods for scattered sample data: accuracy, spatial patterns, processing time. Cartography and Geographical Information Systems 23 (3), 128–144.

Desmet, P.J.J., 1997. Effects of interpolation errors on the analysis of DEMs. Earth Surface Processes and Landforms 22, 563–580.

Erdogan, S., 2009. A comparison of interpolation methods for producing digital elevation models at the fields scale. Earth Surface Processes Landforms 34, 366–376.

Evans, R., 2003. Current themes, issues and challenges concerning the prediction of subsurface conditions. In: Rosenbaum, M.S., Turner, A.K. (Eds.), New paradigms in subsurface prediction: characterization of the shallow subsurface: implications for urban infrastructure and environmental assessment. Springer, Düsseldorf, pp. 359–378.

Fisher, P.F., Tate, N.J., 2006. Causes and consequences of error in digital elevation models. Progress in Physical Geography 30 (4), 467–489.

Flageollet, J.-C., Malet, J.-P., Maquaire, O., 2000. The 3D structure of the Super Sauze earth flow: a first stage towards modelling its behaviour. Physics and Chemistry of the Earth 25 (9), 785–791.

Gallerini, G., De Donatis, M., 2009. 3D modeling using geognostic data: the case of the low valley of Foglia river (Italy). Computer & Geosciences 35, 146–164.

Genet, J., Malet, J.-P., 1997. Détermination de la structure tridimensionnelle du glissement de terrain de Super-Sauze par une investigation géotechnique, Master Thesis, University Louis Pasteur, Strasbourg, France, 138 pp.

Golden Software, 2002. Chapter 4: Creating grid files. Surfer 8 contouring and 3D surface mapping for scientists and engineers user's guide. Golden Software, Golden.

Grandjean, G., Malet, J.-P., Bitri, A., Méric, O., 2007. Geophysical data fusion by fuzzy logic for imaging the mechanical behaviour of mudslides. Bulletin de la Société Géologique de France 178 (2), 127–136.

Gundogdu, K.S., Guney, I., 2007. Spatial analysis of groundwater levels using universal kriging. Journal Earth System Sciences 116 (1), 49–55.

Hengl, T., 2006. Finding the right pixel size. Computer & Geosciences 32, 1283–1298.

Jaboyedoff, M., Couture, R., Locat, P., 2009. Structural analysis of Turtle Mountain (Alberta) using digital elevation model: toward a progressive failure. Geomorphology 103, 5–16.

Jongmans, D., Garambois, S., 2007. Geophysical investigation of landslides: a review. Bulletin de la Société Géologique de France 2, 101–112.

Jones, R.R., McCaffrey, K.J.W., Clegg, P., Wilson, R.W., Holliman, N.S., Holdsworth, R.E., Imber, J., Waggott, S., 2009. Integration of regional to outcrop digital data: 3D visualization of multi-scale geological models. Computer & Geosciences 35, 4–18.

Jordan, G., 2006. Adaptive smoothing of valleys in DEMs using TIN interpolation from ridgeline elevations: an application to morphotectonic aspect analysis. Computer & Geosciences 33, 573–585.

Kalenchuk, K.S., Hutchinson, D.J., Diederichs, M.S., 2009. Application of spatial prediction techniques to defining three-dimensional shear surface geometry. Landslide 6, 321–333.

Kaufmann, O., Martin, T., 2008. 3D geological modelling from boreholes, cross-sections and geological maps, application over former natural gas storages in coal mines. Computer & Geosciences 34, 278–290.

Kienzle, S., 2004. The effect of DEM raster resolution on first order, second order and compound terrain derivatives. Transactions in GIS 8 (1), 83–112.

Lee, D.T., Schachter, B.J., 1980. Two algorithms for constructing a Delaunay triangulation. International Journal of Computer and Information Sciences 9 (3), 219–242.

Lelièvre, P., Oldenburg, D., Williams, N., 2008. Constraining geophysical inversions with geologic information. SEG technical program expanded abstracts 27 (1), 1223–1227.

Maerten, L., Maerten, F., 2006. Chronologic modeling of faulted and fractured reservoirs using geomechanically based restoration; technique and industry applications. Bulletin of the American Association of Petroleum Geologists 90 (8), 1201–1226.

Malet, J.-P., Maquaire, O., Calais, E., 2002. The use of global positioning system for the continuous monitoring of landslides. Application to the Super-Sauze earthflow (Alpes-de-Haute- Provence, France). Geomorphology 43, 33–54.

Malet, J.-P., Remaître, A., Maquaire, O., Ancey, C., Locat, J., 2003. Flow susceptibility of heterogeneous marly formations. Implications for torrent hazard control in the Barcelonnette basin (Alpes-de-Haute-Provence, France). In: Rickenmann, D., Chen, C.-L. (Eds.), Proceedings of the Third International Conference on Debris flow Hazard Mitigation: Mechanics, Prediction and Assessment, Davos. Millpress, Rotterdam, Switzerland, pp. 351–362.

Malet, J.-P., 2003. Les glissements de type écoulement dans les marnes noires des Alpes du Sud. Morphologie, fonctionnement et modélisation hydromécanique. PhD Thesis in Earth Sciences, Université Louis Pasteur, Strasbourg, 364 pp.

Mallet, J.-L., 2004. Space-time mathematical framework for sedimentary geology. Mathematical Geology 36 (1), 1–32.

Marinoni, O., 2003. Improving geological models using a combined ordinary-indicator kriging approach. Engineering Geology 69, 37–45.

Martelet, G., Calcagno, P., Gumiaux, C., Truffert, C., Bitri, A., Gapais, D., Brun, J.P., 2004. Integrated 3D geophysical and geological modeling of the Hercynian Suture Zone in the Champtoceaux area (south Brittany, France). Tectonophysics 382, 117–128.

McKean, J., Roering, J., 2004. Objective landslide detection and surface morphology mapping using high-resolution airborne laser altimetry. Geomorphology 57, 331–351.

Méric, O., Garambois, S., Malet, J.-P., Cadet, H., Gueguen, P., Jongmans, D., 2007. Seismic noise-based methods for soft-rock landslide characterization. Bulletin de la Société Géologique de France 178 (2), 137–148.

Moretti, I., 2008. Working in complex areas: new restoration workflow based on quality control, 2D and 3D restorations. Marine and Petroleum Geology 25 (3), 205–218.

Oppikofer, T., Jaboyedoff, M., Blikra, L., Derron, M.-H., Metzger, R., 2009. Characterization and monitoring of the Aknes rockslide using terrestrial laser scanning. Natural Hazards and Earth System Sciences 9, 1003–1019.

Picarelli, L., Russo, C., Urcioli, G., 1995. Modelling earthflow movement based on experiences. Proceedings of the 11th European Conference on Soil Mechanics and Foundation Engineering, Copenhagen, Balkema, pp. 157–162.

Picarelli, L., 2001. Transition from slide to earthflow, and the reverse. Proceedings of the Conference on Transition from Slide to Flow-Mechanisms and Remedial Measures. Karadeniz Technical University, Trabzon, Turkey.

Picarelli, L., Urciuoli, G., Ramondini, M., Comegna, L., 2005. Main features of mudslides in tectonised highly fissured clay shales. Landslides 2, 15–30.

Poeter, E.P., Mckenna, S.A., 1995. Reducing uncertainty associated with groundwater-flow and transport predictions. Ground Water 33 (6), 899–904.

Regli, C., Rosenthaler, L., Huggenberger, P., 2004. GEOSSAV: a simulation tool for subsurface applications. Computer & Geosciences 30, 221–238.

Rockworks, 2004. Rockworks software documentation. Available at www.rockware.com.

Royle, A.G., Clausen, F.L., Frederiksen, P., 1981. Practical universal kriging and automatic contouring. Geoprocessing 1, 377–394.

Savage, W.Z., Smith, W.K., 1986. A model for the plastic flow of landslides. US Geological Survey Professional Paper 1385 32 pp.

Savage, W.Z., Wasowski, J., 2006. A plastic flow model for the Acquara-Vadoncello landslide in Senerchia, Southern Italy. Engineering Geology 83, 4–21.

Shannon, C.E., 1949. Communication in the presence of noise. Proceedings of the Institute of Radio Engineers 37 (1), 10–21.

Sharma, P.V., 1997. Environmental and Engineering Geophysics. Cambridge Univ. Press, New York. 475 pp.

Schmutz, M., Albouy, Y., Guérin, R., Maquaire, O., Vassal, J., Schott, J.-J., Descloîtres, M., 2001. Joint electrical and Time Domain Electromagnetism (TDEM) data inversion applied to the Super Sauze earthflow (France). Surveys in Geophysics 4, 371–390.

Schmutz, M., Guérin, R., Andrieux, P., Maquaire, O., 2009. Determination of the 3D structure of an earthflow by geophysical methods: the case of Super Sauze, in the French southern Alps. Journal of Applied Geophysics 68 (4), 500–507.

Schulz, W.H., McKenna, J.P., Kibler, J.D., Biavati, G., 2009. Relations between hydrology and velocity of a continuously moving landslide — evidence of pore-pressure feedback regulating landslide motion? Landslides 6, 181–190.

Sowers, G.F., Royster, D.L., 1978. Field Investigation, in Landslide Analysis and Control. In: Schuster, R.L., Krizek, R.J. (Eds.), Special report 176. National Academy of Sciences, Washington. 234 pp.

Squarzoni, C., Delacourt, C., Allemand, P., 2003. Nine years of spatial and temporal evolution of the La Valette landslide observed by SAR interferometry. Engineering Geology 68, 53–66.

Teza, G., Pesci, A., Genevois, R., Galgaro, A., 2008. Characterization of landslide ground surface kinematics from terrestrial scanning and strain field computation. Geomorphology 97, 424–437.

Travelletti, J., Oppikofer, T., Delacourt, C., Malet, J.-P., Jaboyedoff, M., 2008. Monitoring landslides displacements during a controlled rain experiment using a long-range terrestrial laser scanning (TLS). The International Archives of the Photogrammetry, Remote Sensing and Spatial Information Sciences, Vol. XXXVII, pp. 485–490. Part B5.

Travelletti, J., Malet, J.-P., Hibert, C., Grandjean, G., 2009. Integration of geomorphological, geophysical and geotechnical data to define the 3D morpho-structure of the La Valette mudslide (Ubaye Valley, French Alps). In: Malet, J.-P., Remaître, A., Boogard, T. (Eds.), Proceedings of the international conference on landslide processes: from geomorphologic mapping to dynamic modelling, Strasbourg, CERG Editions, pp. 203–208.

Turner, A.K., Schuster, R.L., 1996. Landslides-investigations and mitigation. Transportation Research, 247. National Academy of Sciences, Washington D.C. Board Special Report.

van Asch, Th.W.J., Malet, J.-P., van Beek, L.P.H., 2006. Influence of landslide geometry and kinematic deformation to describe the liquefaction of landslides: Some theoretical considerations. Engineering Geology 88, 59–69.

van Den Eeckhaut, M., Poesen, J., Verstraeten, G., Vanacker, V., Moeyersons, J., Nyssen, J., van Beek, L.P.H., 2005. The effectiveness of hillshade maps and expert knowledge in mapping old deep-seated landslides. Geomorphology 67, 351–363.

Varnes, D.J., Smith, W.K., Savage, W.Z., Powers, P.S., 1996. Deformation and control surveys: Slumgullion landslide. U.S. Geological Survey Bulletin 2130, 43–49.

Weber, D., Herrmann, A., 2000. Contribution of digital photogrammetry in spatio-temporal knowledge of unstable slopes: the example of the Super-Sauze landslide (Alpes-de-Haute-Provence, France). Bulletin de la Société Géologique de France 171, 637–648.

Weng, Q., 2006. An evaluation of spatial interpolation accuracy of elevation data. In: Riedl, A., Kainz, W., Elmes, G.A. (Eds.), Progress in Spatial Data Handling. Springer-Verlag, Berlin, pp. 805–824.

Zimmerman, D., Pavlik, C., Ruggles, A., Armstrong, M., 1999. An experimental comparison of ordinary and universal kriging and inverse distance weighting. Mathematical Geology 31, 375–390.